A&A 562, A135 (2014)
DOI: 10.1051/0004-6361/201322758

Astronomy & Astrophysics

The IACOB project⋆,⋆⋆

I. Rotational velocities in northern Galactic O- and early B-type stars revisited. The impact of other sources of line-broadening

S. Simón-Díaz[1,2] and A. Herrero[1,2]

[1] Instituto de Astrofísica de Canarias, 38200 La Laguna, Tenerife, Spain
e-mail: ssimon@iac.es
[2] Departamento de Astrofísica, Universidad de La Laguna, 38205 La Laguna, Tenerife, Spain

Received 27 September 2013 / Accepted 15 November 2013

ABSTRACT

Context. Stellar rotation is an important parameter in the evolution of massive stars. Accurate and reliable measurements of projected rotational velocities in large samples of OB stars are crucial to confront the predictions of stellar evolutionary models with observational constraints.

Aims. We reassess previous determinations of projected rotational velocities ($v \sin i$) in Galactic OB stars using a large, high-quality spectroscopic dataset and a strategy that accounts for other sources of line-broadening in addition to rotation.

Methods. We present a versatile and user-friendly IDL tool – based on a combined Fourier transform (FT) + goodness-of-fit (GOF) methodology – for the line-broadening characterization in OB-type stars. We used this tool to (a) investigate the impact of macroturbulent and microturbulent broadenings on $v \sin i$ measurements, and (b) determine $v \sin i$ and the size of the macroturbulent broadening ($v_{\rm m}$) in a sample of ∼200 Galactic OB-type stars.

Results. We present observational evidence that illustrates the strengths and limitations of the proposed FT+GOF methodology for OB stars. We confirm previous statements (that were based on indirect arguments or smaller samples) that the macroturbulent broadening is ubiquitous in the massive-star domain. We compare the newly derived $v \sin i$ for O stars and early-B supergiants and giants (where the effect of macroturbulence was found to be stronger) with previous determinations that did not account for this additional line-broadening contribution, and show that cases with $v \sin i \leq 120$ km s^{-1}need to be systematically revised downward by ∼25 (±20) km s^{-1}. We suggest that microturbulence may impose an upper limit below which $v \sin i$ and $v_{\rm m}$ may be incorrectly derived by means of the proposed methodology as it is currently used, and discuss the implications of this statement on the study of relatively narrow-line massive stars.

Conclusions. An investigation of the impact of the revised $v \sin i$ distributions on the predictions of massive star evolutionary models is now warranted. The reliability of $v \sin i$ measurements in the low $v \sin i$ regime, using a more precise description of the intrinsic profiles that are employed for the line-broadening analysis, also needs to be investigated in more detail.

Key words. stars: early-type – stars: rotation – techniques: spectroscopic – line: profiles – astronomical databases: miscellaneous

1. Introduction

The stellar mass is the primary parameter in determining the structure and evolution of a star and, traditionally, the chemical composition (viz. metallicity) has been considered as the second-most relevant parameter. However, it has been 15 years since Maeder & Meynet (2000) highlighted that rotation is indispensable for a proper modeling of the evolution for the upper main sequence stars in their review about the evolution of rotating massive stars (see also the more recent review by Langer 2012, and references in both documents). Thanks to these and subsequent related studies we know that rotation in massive stars may play a role comparable to that of mass and metallicity in our interpretation of the position occupied by these stars in the Hertzsprung-Russell diagram. Moreover, accounting for the effects of rotation (including rotational mixing) in massive-star models has been crucial for investigating (a) the surface abundance pattern observed in massive stars (e.g Hunter et al. 2009; Przybilla et al. 2010; Bouret et al. 2013); and (b) the effect of very extreme rotation in their evolution[1] and final fate (long-duration gamma-ray burst and hypernovae, peculiar bright Type II and Type Ib/c supernovae, e.g., Georgy et al. 2009; Langer 2012).

Even more recent works show the importance of binary interactions for the evolution of massive stars and for the interpretation of population observations and synthesis population calculations (see Sana et al. 2012; de Mink et al. 2013, and references therein). These studies reveal that the present stellar rotation rate is a key parameter indicative of the past history of the binary systems.

All the predictions by rotating stellar evolution models must always be supported by observational constraints. Ideally, we

⋆ Based on observations made with the Nordic Optical Telescope, operated on the island of La Palma jointly by Denmark, Finland, Iceland, Norway, and Sweden, in the Spanish Observatorio del Roque de los Muchachos of the Instituto de Astrofísica de Canarias.

⋆⋆ Appendix A is available in electronic form at http://www.aanda.org

[1] Extreme rotation is predicted to be responsible for homogeneous evolution (Maeder 1987), in which the inner distribution of angular momentum is importantly affected from the very early evolutionary stages.

would like to know the initial distribution of rotational velocities and their temporal evolution as a function of the other stellar properties (mass, luminosity, metallicity, multiplicity, etc.). However, what we can actually measure is the projected rotational velocity ($v \sin i$) of a certain star at given instant in its life. Therefore, to compensate this observational deficiency, $v \sin i$ measurements of large samples of O- and early-B main-sequence stars, as well as B supergiants (B Sgs) are of ultimate importance for our understanding of the massive stars and the stellar populations that include them (and that they often dominate).

One of the most straightforward and cheapest (from an observational point of view) ways to obtain information about (projected) rotational velocities in stars is based on the effect that rotation produces on the spectral line profiles (i.e., line-broadening). Following this approach, the analysis of large samples of Galactic O- and early-B type stars via linewidth measurements (e.g., Slettebak 1956; Conti & Ebbets 1977) or cross-correlation techniques (e.g., Penny 1996; Howarth et al. 1997) provided a general overview of the rotational properties of stars in the upper part of the Hertzprung-Russell diagram.

The $v \sin i$ measurements in all these works were, however, obtained under the assumption that rotation is the sole source of broadening. While the quantification of the global line-broadening is a relatively easy task, the translation of these quantities into actual projected rotational velocities for O- and B-type stars may become complex in certain situations (see, e.g., some notes in Howarth 2004, and references therein). The determination of actual $v \sin i$ becomes even more complicated with the increasing evidence that rotation is not the only broadening mechanism that shapes the line-profiles of these stars. More than 70 years ago, Struve (1952) provided several convincing arguments against a strict rotational interpretation of line-broadening in this class of stars. Slettebak (1956), Conti & Ebbets (1977), Penny (1996), and Howarth et al. (1997) also supported this statement based on the lack of O-type stars and early-B Sgs with sharp absorption lines among the large samples analyzed. More recently, the advent of high-quality spectroscopic observations (in terms of resolving power and signal-to-noise ratio) and their analysis by means of adequate techniques (e.g., Ryans et al. 2002; Simón-Díaz & Herrero 2007) has allowed us to confirm the presence of an additional broadening mechanism that shapes the line-profiles of these types of stars. It was called macroturbulent broadening at some point; however, it is easy to discard that this additional broadening is produced by any type of large-scale turbulent motion (Simón-Díaz et al. 2010). Nevertheless, for the sake of simplicity, we retain the name macroturbulence here.

After the hypotheses by Struve were confirmed, several questions needed to be answered. Is it possible to distinguish the two broadening contributions from the line profiles? How are previous determinations of projected rotational velocities affected? And last, but not least, what is the physical origin of the anomalous non rotational broadening?.

The past decade has witnessed good progress in the investigation of all these questions, especially for B Sgs (e.g., Dufton et al. 2006; Lefever et al. 2007; Markova & Puls 2008; Aerts et al. 2009; Fraser et al. 2010; Simón-Díaz et al. 2010). However, a complete understanding of the impact of macroturbulent broadening in the whole massive-star domain requires a comprehensive, homogeneous analysis of a large sample of high-quality spectra of OB stars, also including early-B dwarfs and giants and, of course, O-type stars of all luminosity classes. This was one of the initial objectives of the IACOB project (P.I. Simón-Díaz), which aims at progressing in our knowledge of Galactic massive stars using a large, homogeneous, high-quality spectroscopic dataset and modern tools for the quantitative spectroscopic analysis of O- and B-type stars.

Some preliminary results concerning the study of the projected rotational velocities and the macroturbulent broadening in the IACOB sample can be found in Simón-Díaz et al. (2012), and references therein. Here, we present the complete study for the first time, also including a detailed description of the strengths and limitations of the methodology we have applied to distinguish the two broadening contributions in a sample of ~200 northern Galactic O- and early-B stars (covering all luminosity classes). In a parallel work to this one, Markova et al. (2014) provided observational constraints on the projected rotational velocities and the amount of macroturbulent broadening as a function of fundamental parameters and stellar evolution from the analysis of a sample of 31 Southern Galactic O stars (own new data) plus 86 OB supergiants from the literature.

The paper is structured as follows: in Sect. 2 a brief description of the spectroscopic dataset used for this study is presented. The strategy we followed for the line-broadening characterization of our sample of O and B stars is described in Sect. 3. Particular emphasis is given to the description of the software we used, the `iacob-broad` tool, a versatile procedure developed and implemented by us in IDL, which provides a complete set of quantities and visual information resulting from a combined Fourier transform plus a goodness-of-fit analysis of the line-broadening in OB stars. The analysis of the whole sample and the discussion of results can be found in Sect. 4, while the main conclusions are summarized in Sect. 5.

2. Observations

The spectroscopic observations considered for this study are part of the IACOB spectroscopic database of northern Galactic OB stars (last described in Simón-Díaz et al. 2011a,b). This unique high-quality spectroscopic database has been compiled in the framework of the IACOB project. To date, the IACOB database comprises 1250 spectra of 153 and 97 Galactic O- and early B-type stars, respectively, observable from the Roque de los Muchachos observatory in La Palma (Spain). The spectra have a resolving power of 46 000 and 23 000, a typical signal-to-noise ratio (S/N) above 150, and were compiled between November 2008 and January 2013 with the high-resolution FIbre-fed Echelle Spectrograph (FIES) attached to the Nordic Optical Telescope (NOT). The IACOB database has a multi-epoch character that enables investigations of the binary/multiple nature of considered stars and the temporal variations in individual objects with at least three spectra per observed target. In this study, we only used a subsample of the spectra, discarding all stars with signatures of multiplicity (which means that we only considered apparently single and SB1 stars), and only considering the spectrum with the highest S/N ratio per star.

All the spectra were homogeneously reduced using the FIES-tool pipeline, revised and normalized using our own procedures developed in IDL. The spectroscopic observation covers the full wavelength range between 3700 and 7000 Å without gaps; however, for this study we only used the spectral windows including the Si III λ4552 and O III λ5592 lines for early-B and O-type stars, respectively.

3. Methods

Motivated by the investigation performed here we developed a versatile and user-friendly IDL tool for the line-broadening

characterization of OB-type spectra: the `iacob-broad`. This procedure allows us to determine $v \sin i$ and the macroturbulent broadening ($v_{\rm m}$) for a variety of situations, and it is based on a combined Fourier transform (FT) + goodness-of-fit (GOF) methodology.

These two methods are (independently) able to separate the rotational broadening contribution to the line profile from other line-broadening components, but they also present some caveats that must be taken into account for a correct interpretation of the results. We have found that a combined use of both techniques helps us to not only provide more reliable final estimates of $v \sin i$ and $v_{\rm m}$ (plus their associated uncertainties), but also to better understand the problematic cases and identify spurious solutions.

While the `iacob-broad` tool has been used in several publications in the past few years (e.g., Simón-Díaz et al. 2010; Degroote et al. 2010; Aerts et al. 2013; Ramírez-Agudelo et al. 2013; Sundqvist et al. 2013; Markova et al. 2014), it has not been formally described yet. In this section, we briefly describe the basics of the tool and explore the strengths and limitations of the proposed methodology. To this aim, we present a couple of formal tests carried out to investigate the effect that the assumed macroturbulent profile has on the GOF-based $v \sin i$ and $v_{\rm m}$ estimates (Sect. 3.3), and the possible consequences of neglecting the effect of microturbulence on the determination of these two quantities (Sect. 3.4).

3.1. The Fourier transform and goodness-of-fit methods in a nutshell

The FT method was first introduced by Carroll (1933) and some years later was revisited and extended by Gray (1976, 2005). This technique is based (in its more simple form) on the identification of the first zero in the Fourier transform of the line-profile, and the direct translation of the associated frequency (σ_1) into the corresponding projected rotational velocity via the formula

$$\frac{\lambda}{c} v \sin i \sigma_1 = 0.660, \quad (1)$$

where λ is the central line wavelength and c is the velocity of light. This technique has been commonly used for cool stars since the pioneering works, for instance, by Wilson (1969), Gray (1973), or Smith & Gray (1976), but has been only marginally applied to early OB-type stars before the first decade of the twenty-first century. After the work by Ebbets (1979), Simón-Díaz & Herrero (2007) first applied this technique in a systematic way to the OB star domain. Since then, the FT method has been increasingly used for the study of this type of stars (e.g., Dufton et al. 2006; Lefever et al. 2007; Hunter et al. 2008; Markova & Puls 2008; Fraser et al. 2010; Lefever et al. 2010; Bouret et al. 2012; Grunhut et al. 2012; Dufton et al. 2013; Ramírez-Agudelo et al. 2013; Markova et al. 2014).

The FT method must be used with particular care when the rotational broadening is comparable to (or smaller than) the resolving power of the spectrum and/or the intrinsic[2] broadening of the line. In addition, three other caveats must be kept in mind when extracting information about $v \sin i$ from the FT of the line-profile: (a) when the so-called macroturbulent broadening is comparable to or larger than the rotational broadening and the S/N ratio of the line is not high enough, the position of the first zero could be hidden below the white-noise in the Fourier space, resulting in an apparent displacement to lower frequencies (i.e. larger $v \sin i$). An example of this effect can be found in Simón-Díaz & Herrero (2007). Moreover, even when the line quality is optimal, we should keep in mind the word of caution indicated by Gray (2005): when macroturbulence dominates over rotation, the sidelobe structure of the Fourier transform may be affected; (b) if the line is asymmetric and/or the final line-profile is not the result of a convolution of the various broadening agents, the first zero of the FT may not be related to the actual projected rotational velocity. An example of this caveat is found in Aerts et al. (2009). If the macroturbulent broadening has a pulsational origin (a possibility investigated by these authors in B Sgs), then $v \sin i$ determinations may be seriously underestimated by using a simple parameter description for macroturbulence instead of an appropriate pulsational model description to fit the line profiles; and c) as indicated by Gray (1973), microturbulent broadening also adds zeroes to the FT at frequencies associated to low $v \sin i$ values, which could be misinterpreted as zeroes produced by rotation (see also discussion in Sect. 3.4).

The goodness-of-fit (GOF) technique is based on a simple line-profile fitting in which an intrinsic profile is convolved with the various considered/investigated line-broadening profiles and compared with the observed profile using a χ^2 formalism. An example of the application of this technique to a sample of Galactic early-B Sgs can be found in Ryans et al. (2002). As pointed out by these authors, one of the caveats of the GOF method in separating rotational from macroturbulent broadening is the high degree of degeneracy in the resulting profiles when convolved with different ($v \sin i$, $v_{\rm m}$) combinations (resulting in a banana-shaped χ^2 distribution, see e.g., Figs.1 and 2). Even more, different descriptions of the macroturbulent profile lead to different $v_{\rm m}$ and $v \sin i$ measurements (see Sect. 3.3). In addition, the derived $v \sin i$ and $v_{\rm m}$ may be erroneous if the total broadening is comparable to the intrinsic broadening of the line and the latter is not properly taken into account. This second warning must especially be kept in mind when using He I-II lines because of the effect of Stark broadening (see e.g., Ramírez-Agudelo et al. 2013), and in stars with relatively low $v \sin i$ and $v_{\rm m}$ (due to the effect of microturbulence, see the detailed discussion in Sect. 3.4).

While the GOF technique allows for the full characterization of the line-broadening in terms of projected rotational and macroturbulent velocities, the identification of the first zero in the FT only provides a measurement of $v \sin i$. The estimation of the extra-broadening in this case requires an additional comparison of synthetic profiles broadened by rotation and macroturbulence and the observed profiles (either in the lambda or Fourier domain). Gray (1976, 2005) proposed the use of the full information contained in the FT of the line-profile. The strategy we follow in this paper is based on a combined FT+GOF approach.

3.2. `iacob-broad`: a combined FT+GOF analysis

The general philosophy of the `iacob-broad` IDL procedure is simple: extract from just one shot as much information as possible about the line-broadening characteristics of a given stellar line-profile in a versatile and user-friendly way. This information is obtained by the combined application of the two methodologies described in the previous subsection to an observed line-profile.

Before starting the combined FT+GOF analysis, the tool allows for a preprocessing of the line profile (e.g., renormalization of the local continuum, clipping part of the line-profile to eliminate nebular contamination) and for the selection of the intrinsic

[2] In this context, the intrinsic line profile includes natural, thermal, and Stark broadening.

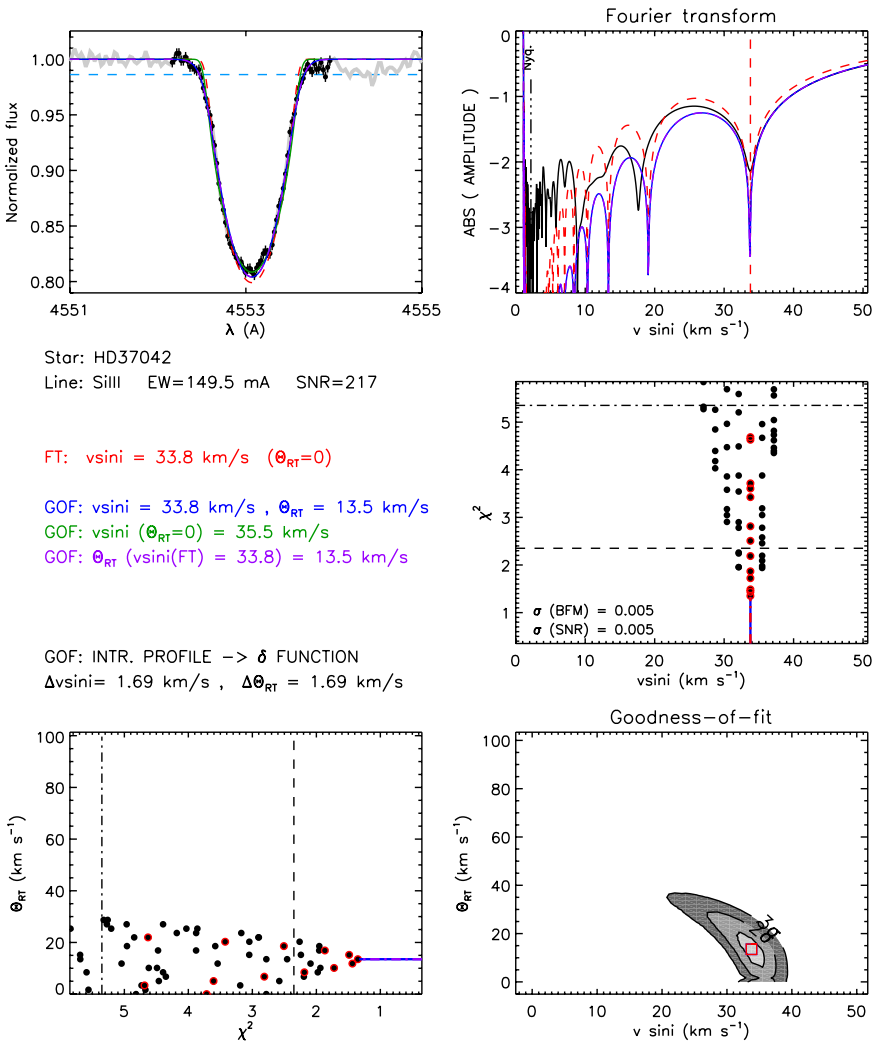

Fig. 1. Example of graphical output from the `iacob-broad` tool for the B0.7 V star HD 37042. Five main graphical results are presented: (a) the line profile (*upper left*); (b) the FT of the line (*upper right*); and (c) 2D χ^2-distributions resulting from the GOF analysis (*lower right*) and their projections (*middle and lower left*). See text for more detailed explanations.

profile (either a delta-function or a line profile from a stellar atmosphere code). For the purposes of the present work, two types of macroturbulent profile were incorporated into the GOF analysis: an isotropic Gaussian, and a radial-tangential description (see Gray 2005, for definitions).

Figures 1 and 2 show the graphical output resulting from the `iacob-broad` analysis of the Si III λ4452 line from the IACOB spectra of HD 37042 (B0.7 V) and HD 91316 (B1 Iab N str.). Each graphical output includes as much information as possible concerning the broadening characterization of the studied line. Five main graphical results are presented: (a) the line profile (upper left); (b) the FT of the line (upper right); and (c) 2D χ^2-distributions resulting from the GOF analysis (lower right) and their projections (above and to the left). In addition, the following information is provided in the same figure (the associated uncertainties are calculated and provided on the screen and output files):

- the $v \sin i$ corresponding to the first zero of the FT;
- the $v \sin i$ and macroturbulent velocity resulting from the GOF, assuming both are free parameters;
- the $v \sin i$ resulting from the GOF, when the macroturbulent velocity is fixed to zero (i.e., this result assumes that the full broadening is due to rotation and is directly comparable with previous studies not accounting from the extra-broadening);
- the macroturbulent velocity resulting from the GOF when the $v \sin i$ is fixed to the value corresponding to the first zero of the FT.

For the sake of simplicity, we denote these different values as $v \sin i$(FT), $v \sin i$(GOF), $v_{\rm m}$(GOF), $v \sin i$(GOF, $v_{\rm m} = 0$), and $v_{\rm m}$(FT+GOF), respectively, throughout the paper. We use $v_{\rm m}$ when we generically refere to macroturbulent velocity. On the other hand, since two different characterizations of this broadening agent are used in this paper, namely an isotropic Gaussian profile and a radial-tangential profile, we quote these two possibilities as $\Theta_{\rm G}$ and $\Theta_{\rm RT}$, respectively.

For each set of resulting broadening parameters, the initially considered synthetic profile is convolved with the ($v \sin i$, $v_{\rm m}$) pair and degraded to the resolving power of the analyzed spectra; then the corresponding profiles and the resulting Fourier transforms are overplotted in the various panels using the same color-code as in the text for better identification.

The graphical output allows the user to understand the impact of the different contributions to the line profile broadening, and evaluate the reliability of the various solutions. From the two examples shown in Figs. 1 and 2, HD 37042 represents a typical case in which rotation dominates the broadening of the Si III line. As a result of this and of the high S/N of the line, the broadening analysis results in an excellent agreement between $v \sin i$(FT) and $v \sin i$(GOF). In addition, $v \sin i$(GOF, $v_{\rm m} = 0$) is very close to these two values. HD 91316, on the other hand, illustrates the case of a star in which an important (dominant) macroturbulent broadening contribution affects the Si III line-profile. In this case, $v \sin i$(FT) = $v$sin(GOF), but inspection of the synthetic line profile and its corresponding FT convolved with this $v \sin i$ value

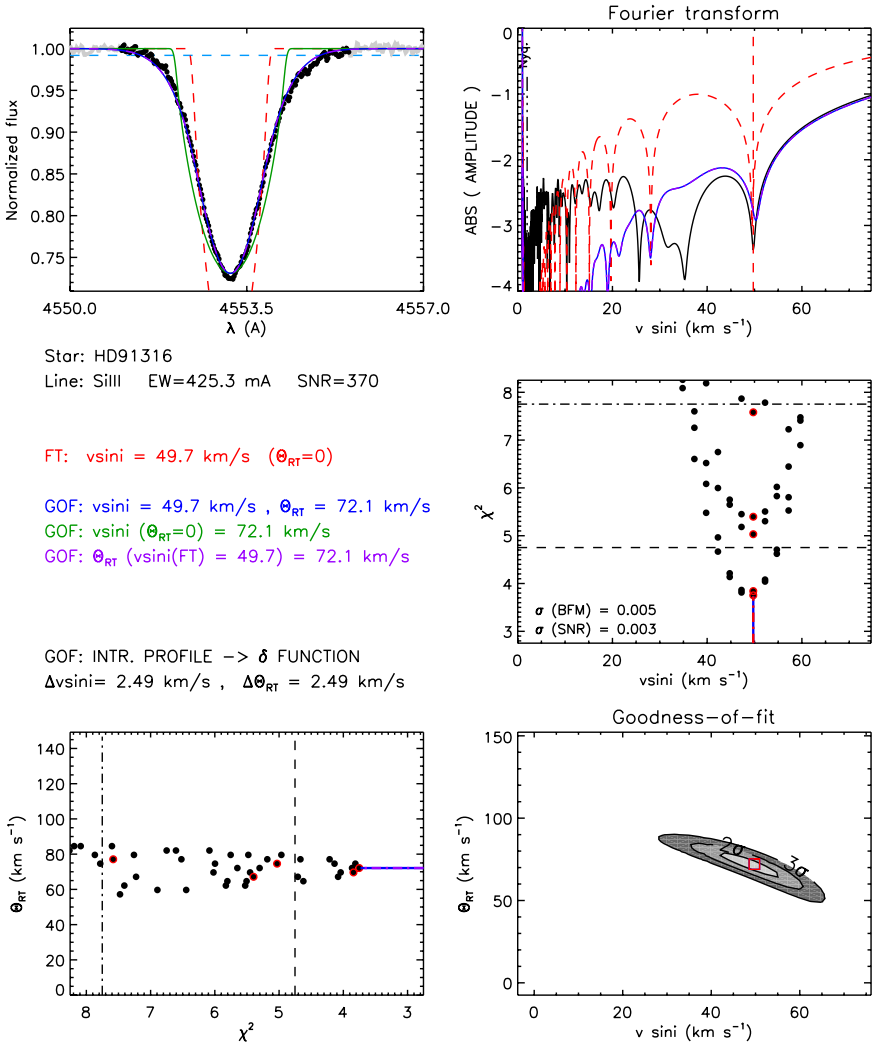

Fig. 2. Same as Fig. 1 for the B1 Iab N str. star HD 91316.

(the red lines in the upper panels of Fig. 2) already tell us that rotation is not the only broadening agent. As a consequence, the derived $v \sin i$ assuming rotation as the only broadening agent results in a too high $v \sin i$ value. We emphasize here the role played by the spectral resolution. At a resolution significantly lower than the present observations ($R = 46\,000$), separating rotation and macroturbulent broadenings would be much more difficult.

These two cases were deliberately selected as examples in which there is perfect agreement between FT and GOF results. However, this will not always be the case. In certain situations, $v \sin i$(FT) $\neq v \sin i$(GOF), and the user will have to use the information provided to decide which one is the correct solution – if any! Some of the possible difficulties are presented in the next subsections.

3.3. Gaussian vs. radial-tangential macroturbulent profile

While the presence of a substantial non rotational broadening has been firmly confirmed (see Sect. 1), its physical origin is still a puzzling question. As a consequence, we still lack a formal description of the corresponding broadening profile. Meanwhile, following some guidelines developed in the context of cool stars, two different definitions of the (up to now so-called) macroturbulent broadening have been commonly used for OB-type stars in the past years: an isotropic Gaussian definition and a radial-tangential definition.

In Simón-Díaz et al. (2010) we pointed out that the values of $v \sin i$ and $v_{\rm m}$ determined by means of the GOF method depend on the assumed macroturbulent profile. There we suggested, based on empirical arguments, that a radial-tangential prescription is more appropriate. In this section we re-assess this topic and provide further evidence that the radial-tangential profile gives more consistent results.

For this investigation we considered a subsample of the IACOB spectra analyzed in this paper that fulfill the following criteria: (a) well-defined zeroes in the FT; (b) $v \sin i \leq 150$ km s^{-1}; and (c) $v_{\rm m} \geq 0.5\, v \sin i$. We carried out the analysis twice, first assuming a radial-tangential profile and then an isotropic Gaussian profile, all other conditions were exactly the same. The upper panel of Fig. 3 compares the $v \sin i$(GOF) values obtained in each case with the corresponding $v \sin i$(FT). While there is a perfect agreement between $v \sin i$(GOF, $\Theta_{\rm RT}$) and $v \sin i$(FT), $v \sin i$(GOF, $\Theta_{\rm G}$) values are systematically too low compared with the FT determinations. The lower panel illustrates the fact that the two different descriptions also lead to different values of $v_{\rm m}$. There is a clear correlation between the $\Theta_{\rm G}$ and $\Theta_{\rm RT}$ measurements, but $\Theta_{\rm G}$ values are systematically lower (~76% for free $v \sin i$ and 65% when $v \sin i$ is fixed to its FT value).

This result is a consequence of the different characteristics of the two profiles. Basically, the isotropic Gaussian profile results in a broader core than the radial-tangential profile for the same wing extension. As a consequence, a lower $v \sin i$ is needed in

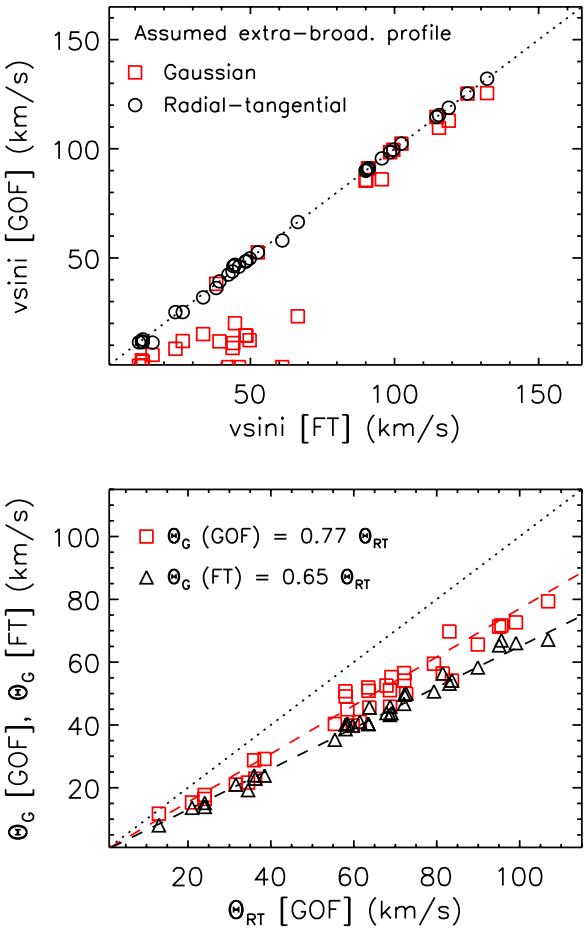

Fig. 3. Comparison of $v \sin i$ and $v_{\rm m}$ estimates resulting from the `iacob-broad` analysis of a subsample of stars $v \sin i \leq 150$ km s^{-1} and $\Theta_{\rm RT} \geq 0.5\, v \sin i$. Two different definitions of the macroturbulent profile are considered in the case of GOF results: an isotropic Gaussian profile and a radial-tangential profile. *Upper panel*: comparison of $v \sin i$ values obtained by means of the FT and GOF techniques. *Lower panel*: comparison of macroturbulent velocities resulting from the GOF analysis. Two options are investigated in the case of the Gaussian profile: (red squares) leaving $v \sin i$ as a free parameter as well; (black triangles) fixing $v \sin i$ to the value provided by the FT. Dotted lines (both panels) represent the one-to-one relation; dashed black and red lines (*bottom panel*) correspond to the linear fit to the data represented as black triangles and red squares, respectively.

the case of the Gaussian profile. This effect is negligible when $v \sin i$ is large enough to dominate the contribution to the line core broadening (see, e.g., the cases with $v \sin i > 100$ km s^{-1} in Fig. 3).

Ryans et al. (2002) were among the first authors who tried to quantify the relative contribution of rotation and macroturbulent broadening in B Sgs. They applied a GOF method with an isotropic Gaussian definition of the macroturbulent profile and concluded that a model where macroturbulence dominates and rotation is negligible is more acceptable than the reverse scenario. Their $v \sin i$ values were, however, too low compared with results obtained afterward based on the Fourier transform. This puzzling result has been neither investigated nor explained in the literature yet. Our investigation definitely explains this discrepancy[3] and shows that $v_{\rm m}$ values from different sources can only be combined with care.

[3] This effect can also be present in some of the more critical cases presented in Figs. 6–8 in Aerts et al. (2009).

Three main conclusions can be extracted from our investigation:

- While the physical origin of the macroturbulent broadening is still unknown (and hence we lack a formal calculation of the profile that describes the additional broadening), the results presented in the upper panel of Fig. 3 support that a radial-tangential macroturbulent profile is better suited to determine rotational velocities in OB stars (based on a GOF approach) than a Gaussian profile.
- The excellent agreement between $v \sin i$(FT) and $v \sin i$(GOF, $\Theta_{\rm RT}$) strengthens the suitability of the FT method for the determination of rotational velocities in OB stars. We also refer to Sects. 3.4 and 4.1 for an in-depth discussion of this statement.
- When investigating relationships between the size of the additional broadening and other stellar parameters, one must combine macroturbulent velocities from the literature with care since there is a systematic offset between values obtained under the various assumptions commonly considered by different authors.

3.4. Effect of microturbulence

In many cases, one has to perform a line-broadening analysis without having access to a realistic intrinsic profile (i.e., computed with a stellar atmosphere code). In that case, it is common to consider a delta-function with the same equivalent width as the observed line. As a consequence, the GOF analysis incorporates all line-broadening not produced by rotation (and spectral resolution) to the $v_{\rm m}$ parameter. One can minimize this effect using metal lines where, in contrast to the case of H and He I-II lines, the Stark broadening is negligible. However, even in this case there is still an important source of line-broadening, which may lead to an overestimation of the macroturbulent broadening: microturbulence.

Microturbulence also has an effect when one performs an FT analysis to determine $v \sin i$. As pointed out by Gray (1973), microturbulence also produces zeroes in the Fourier transform at (high) frequencies associated with low values of $v \sin i$ that may be falsely identified as the zeroes associated with the rotational broadening below a certain $v \sin i$ limit.

In Simón-Díaz & Herrero (2007) we presented a few notes about the effect of microturbulence on the determination of $v \sin i$ via the FT method for OB-type stars. In this section, we extend that study and also investigate the impact that microturbulence can have on our $\Theta_{\rm RT}$ measurements. To this aim, we performed several exercises in which a set of synthetic Si III λ4552 lines computed with the stellar atmosphere code FASTWIND (Santolaya-Rey et al. 1997; Puls et al. 2005) were analyzed using the `iacob-broad` procedure in the same way as the observed spectra. Two values of microturbulence (5 and 20 km s^{-1}) were considered as representative for dwarfs and supergiants, respectively. In a first exercise, each of these two profiles was convolved with different values of $v \sin i$ ranging from 5 to 400 km s^{-1}, and no macroturbulent broadening was incorporated to the synthetic lines. In a second exercise, $v \sin i$ was fixed to 50 km s^{-1} and a macroturbulence ($\Theta_{\rm RT}$) ranging from 10 to 100 km s^{-1} was added to each profile.

Results from these exercises are presented in Figs. 4 and 5, were the derived values of $v \sin i$(FT) and $\Theta_{\rm RT}$(FT+GOF) are compared with the input values. The top panel in Fig. 4 indicates that there is perfect agreement between the derived and the input $v \sin i$ when the first zero associated with rotation is

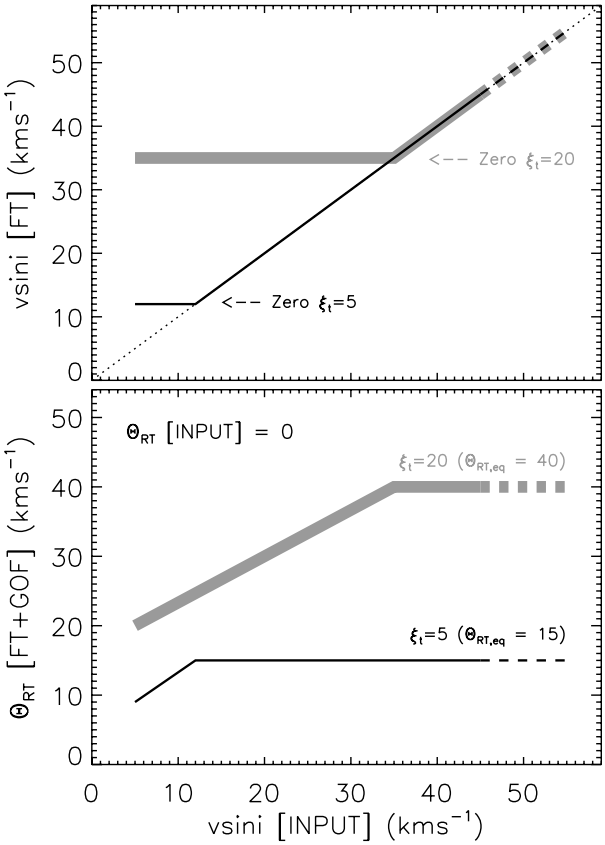

Fig. 4. Effect of microturbulence on the derived $v \sin i$ and Θ_{RT} when microturbulent broadening is not taken into account in the FT+GOF analysis. Black and gray curves indicate the derived broadening parameters resulting from the FT+GOF analysis of a Si III line synthesized assuming two different values of microturbulence (5 and 20 km s^{-1}, respectively). *Top panel*: derived (via FT) vs. input $v \sin i$ values. The positions of the zeroes associated with microturbulence are also indicated. *Bottom panel*: derived Θ_{RT} values for the range of considered input $v \sin i$ values.

located at lower frequencies (larger $v \sin i$) than the zero resulting from microturbulence. On the other hand, for lower $v \sin i$ values the latter would be falsely attributed to rotation and hence the plateau in the derived $v \sin i$. Therefore, microturbulence imposes an upper limit below which $v \sin i$ cannot be correctly derived by means of the first zero in the FT. It is important to note that this $v \sin i$ limit depends on the value of the microturbulence and the equivalent width of the line. The larger these parameters, the higher the limit on the detectable $v \sin i$. In the case of the example considered in Fig. 4, this limit can be up to 35 km s^{-1} for the case of ξ_t = 20 km s^{-1}.

Interestingly, the derived $v \sin i$(GOF) values agree with $v \sin i$(FT) determinations for all the cases considered in these exercises – even when they are false! This seems to indicate that in the low $v \sin i$ regime, when microturbulent broadening dominates, the profile associated to microturbulence (at least in the form resulting from FASTWIND computations) can be mimicked by a rotational profile with a given $v \sin i$ (plus the inclusion of some additional broadening to fit the extended wings on the line).

The lower panel of Fig. 4, along with Fig. 5, illustrates that as expected, a simple $v \sin i + \Theta_{RT}$ analysis without accounting for the effect of microturbulence on the line-profile systematically leads to an overestimation of Θ_{RT}. This effect is more important when the relative contribution of microturbulence vs.

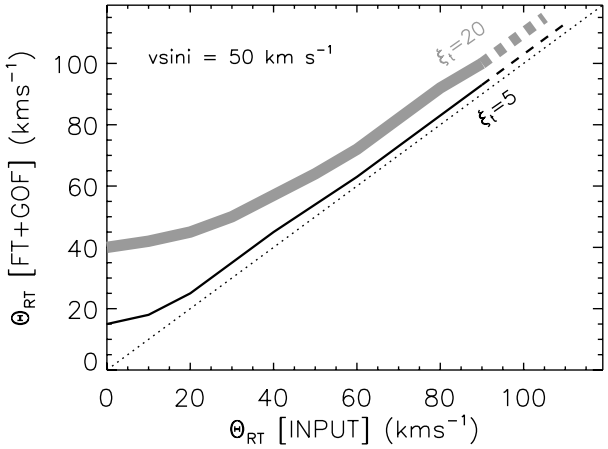

Fig. 5. Effect of microturbulence on the derived Θ_{RT} when microturbulent broadening is not taken into account in the FT+GOF analysis. Black and gray curves indicate the derived Θ_{RT} resulting from the FT+GOF analysis of a Si III line synthesized assuming two different values of microturbulence (5 and 20 km s^{-1}, respectively) and convolved to a fixed $v \sin i$ = 50 km s^{-1}, and the Θ_{RT} values indicated in abscissa.

macroturbulence is larger. In the example considered in the bottom panel of Fig. 4, a microturbulence of 5/20 km s^{-1} in a star without any macroturbulent broadening contribution, could be erroneously interpreted as having $\Theta_{RT} \sim$ 15/40 km s^{-1}, respectively. As indicated in Fig. 5, the relative overestimation decreases with increasing macroturbulence. Interestingly, the input macroturbulence is not perfectly recovered even at high values of Θ_{RT}.

Two main conclusions can be drawn from our study. If the effects of microturbulence are not taken into account,

a) any $v \sin i$ measurement (either from FT or GOF) below ~40 km s^{-1} must be considered as an upper limit (especially for O and early-B Sgs, where the high values of microturbulence are commonly found);
b) any Θ_{RT}(GOF) measurement must be considered as an upper limit of the actual macroturbulent broadening. In particular when $\Theta_{RT} \leq$ 15/40 km s^{-1} in dwarfs/supergiants, the derived macroturbulent broadening may be actually produced by microturbulence; on the other hand, even Θ_{RT} values above 25/60 km s^{-1} may be actually lower by 5/15 km s^{-1}.

We note that all the numbers indicated above must be considered as illustrative since the actual values depend of the equivalent width of the investigated line and the specific microturbulence derived for the star under study.

The two exercises presented in this section warn us about the limitations of the proposed FT+GOF strategy. These warnings are especially important when interpreting results in the low $v \sin i$ and Θ_{RT} regimes and also when the derived line-broadening parameters (specially Θ_{RT}) are used for the spectroscopic determination of the stellar parameters and/or abundances by fitting metal lines. In that case, these values will have to be corrected downward depending on the derived or assumed microturbulence.

Some of these limitations may be overcome if lines with different equivalent widths are analyzed (for the case of $v \sin i$), more zeroes are considered in the FT, and synthetic lines incorporating the microturbulence resulting from a quantitative spectroscopic analysis are considered as initial profiles in the fitting

procedure (for the case of Θ_{RT}). We plan to explore these ways for future improvements.

3.5. Applicability and limitations in the IACOB sample

Before presenting the results of the line-broadening analysis of the whole sample of Galactic OB stars considered in this study (Sect. 4), we summarize below some important points (in addition to the more general ones indicated in previous sections) that must be remembered to correctly interpret the results from the `iacob-broad` analysis of the IACOB spectra.

3.5.1. Resolution and spectral sampling

The resolving power of the IACOB spectra is 46 000 and 25 000 (FIES medium and low-resolution modes, respectively), both having a spectral dispersion of 0.025 Å/pix. The lower $v \sin i$ limit detectable via FT (related to the Nyquist frequency, see Simón-Díaz & Herrero 2007) is ~2 km s^{-1}, and the velocity corresponding to the spectral resolutions is ~5 and ~10 km s^{-1}, respectively.

3.5.2. Signal-to-noise ratio

The S/N of the continuum adjacent to the analyzed lines is typically higher than 150. There are, however, a few cases with an S/N slightly lower than 100.

To investigate the effect of noise for the specific case of the spectroscopic dataset analyzed in this study, we obtained 13 spectra of HD 91316 (one of the examples presented in Sect. 3, see also Fig. 2) with varying exposure times, leading to S/N ranging from 90 to 300. The corresponding Si III λ4552 lines were analyzed with the `iacob-broad` procedure using the same wavelength limits. We found that the derived $v \sin i$(FT) and $v \sin i$(GOF, Θ_{RT}) values range between 36–53, and 41–51 km s^{-1}, respectively, without a clear correlation with the S/N of the continuum. The mean values and standard deviations in each case are 46 ± 5 and 46 ± 3 km s^{-1}, respectively. Therefore, from this single experiment we can conclude that for this spectroscopic dataset, the effect of noise on the derived $v \sin i$ and Θ_{RT} does not seem more relevant than other sources of uncertainty (e.g., local renormalization, asymmetry of the line, undetected spectroscopic binarity).

3.5.3. Broad-line stars

Stars with projected rotational velocities higher than ~150 km s^{-1} deserve a separate section, since they present some problems that are not equally important in more narrow-line stars. The main problems are summarized below.

- The first problem is the possibility of undetected spectroscopic binaries or multiple systems, especially when the various components have large $v \sin i$ and the radial velocity amplitude of the system is small.
- Lines can be really shallow in very fast rotators, and the effect of noise, blending, and especially continuum normalization becomes significant. Above a certain $v \sin i$ value the effect of the additional broadening only results in a subtle shaping of the extended wings (see e.g., Fig. 6), and hence a reliable measurement of Θ_{RT} becomes difficult due to the effect of noise and local continuum normalization on the fitting process. We have found from our analysis that in stars with $v \sin i \geq 180$ km s^{-1} the values of Θ_{RT} resulting from the `iacob-broad` analysis must be considered as upper limits.
- Equatorial gravity-darkening will produce an obscuration of the profile wings associated with the higher velocities and thus an underestimation of the actual $v \sin i$ (Townsend et al. 2004; Frémat et al. 2005). While we here present $v \sin i$ measurements for stars higher than 200 km s^{-1} obtained in the same way as the global sample and without incorporating any correction, we plan to investigate this type of effects in a future paper, also including $v \sin i$ measurements provided by the stronger He I-II lines.

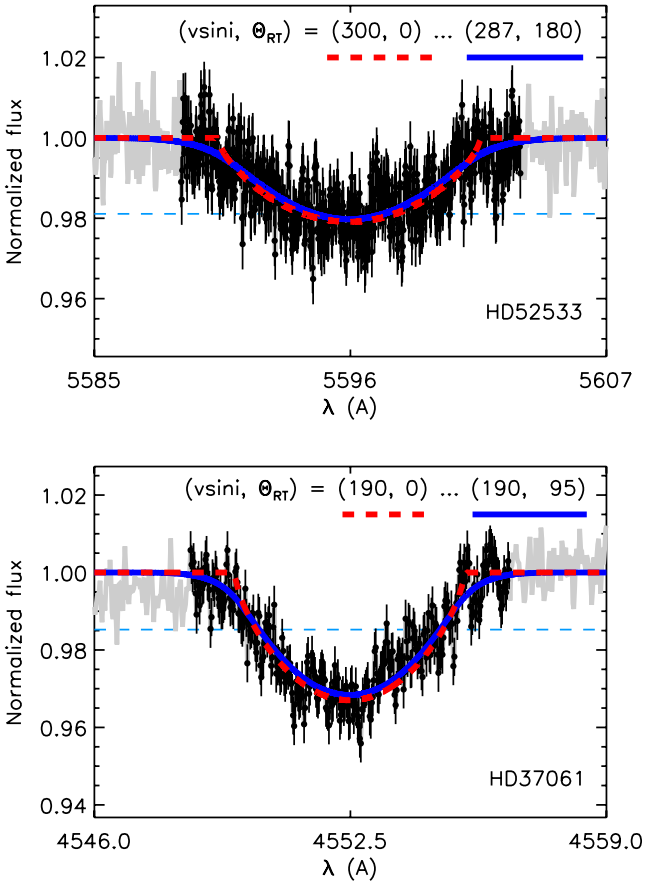

Fig. 6. Representative examples of broad-line stars. In both cases the noise makes the accurate measurement of Θ_{RT} difficult and, in fact, a model with $\Theta_{RT} = 0$ could perfectly fit the line as well. Note that for HD 52533, the increased additional broadening forces $v \sin i$ to be lower than $v \sin i$(FT).

4. Analysis of a sample of northern Galactic OB-type stars

Tables A.1–A.4 summarize the results from the line-broadening characterization of the complete sample. The `iacob-broad` procedure was applied to the O III λ5591 or Si III λ4552 lines depending on the spectral type and luminosity class[4], and the derived $v \sin i$(FT), $v \sin i$(GOF), and Θ_{RT}(GOF) are indicated in Cols. 7–9. The tables also include information about the spectral type and luminosity class of the stars (Cols. 2 and 3), the

[4] There is a small subsample of O9-B0 stars in which the two lines are available. We have found a very good agreement between results from the `iacob-broad` analysis of both lines.

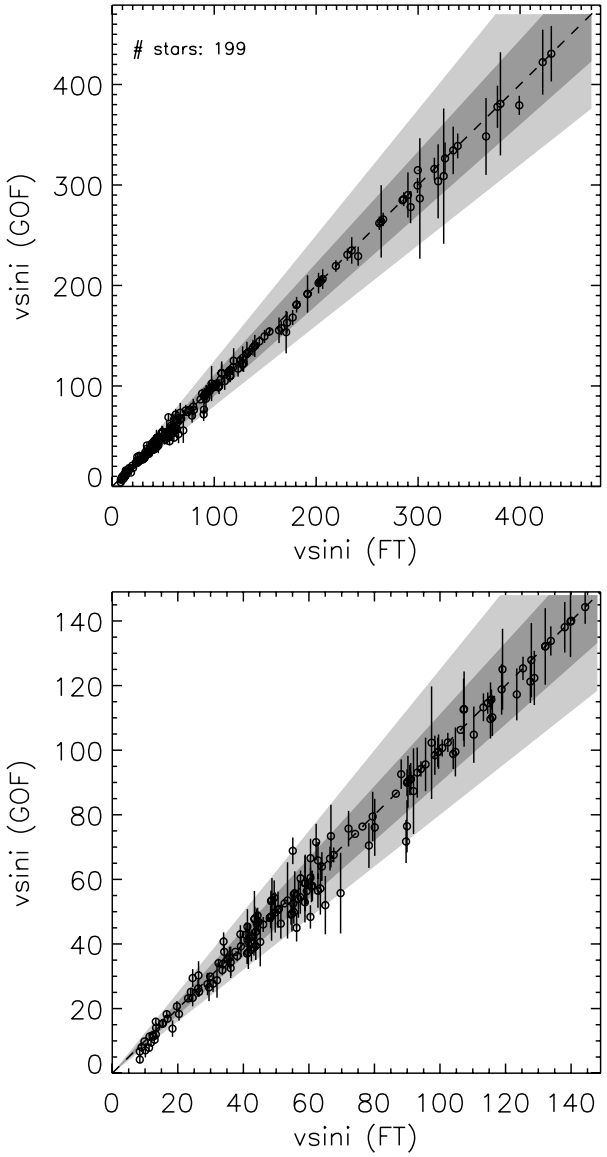

Fig. 7. Comparison of $v \sin i$ measurements derived by means of the FT and GOF techniques. *Upper panel*: full $v \sin i$ range. *Lower panel*: zoom on the low $v \sin i$ range.

used line and its equivalent width (Cols. 4 and 5), and the S/N of the adjacent continuum.

Following the results of the exercise presented in Sect. 3.3, we assumed a radial-tangential definition of the macroturbulent profile. Moreover, we assumed a delta-function as intrinsic profile[5]; therefore, the derived macroturbulence includes all sources of non-rotational broadening (i.e. microturbulence and any other possible unknown source of broadening). This may have important consequences for the cases in which a low value of $v \sin i$ and/or macroturbulence is obtained (see notes in Sect. 3.4).

4.1. v sin i(FT) vs. v sin i(GOF)

Figure 7 compares the $v \sin i$ measurements obtained by means of the FT and GOF approaches. The one-to-one relation is indicated with a dashed line along with the 10% and 20% difference regions in dark and light gray, respectively. The upper panel includes all cases, while the lower panel zooms into the region with $v \sin i$(FT) $\leq$ 150 km s^{-1}. Both $v \sin i$ measurements agree very well (<10%) for all stars with $v \sin i \geq$ 100 km s^{-1}. The situation becomes slightly worse for stars with projected rotational velocities below this limit. The agreement is, however, always better than 20%, except for a few cases with $v \sin i$ measurements below 20 km s^{-1}. Taking into account the results of the exercises presented in Sect. 3.4, all $v \sin i$ values below ~15–35 km s^{-1} must be considered as upper limits (especially in the case of Sgs); hence, cases that disagree in more than 20% in this low $v \sin i$ region can be naturally explained as due to the limitations of our methodology.

Only a small fraction of objects (7 out of the 200 analyzed stars with $v \sin i \geq$ 35 km s^{-1}) present differences between $v \sin i$(GOF) and $v \sin i$(FT) in the range 10–20%. We have explored these cases in more detail and found that most of them correspond to lines affected by a significant macroturbulent broadening contribution (some of them are also slightly asymmetric) in which the first zero of the FT is not sharply defined. Although we cannot exclude other possible effects, the combination of large Θ_{RT} plus an insufficiently high enough S/N can play an important role in the $v \sin i$(FT) determination. As a consequence, most of these cases result in $v \sin i$(FT) slightly larger than $v \sin i$(GOF, Θ_{RT}).

The very good agreement in the derived projected rotational velocities obtained by means of two independent methods can be considered as observational evidence of the strength of both the FT and GOF methodologies. In particular, it allows us to reassess the reliability of the FT method after the word of caution indicated by Aerts et al. (2009). Although we cannot completely discard that the effect described by these authors (see also Sect. 3.1) is absent from our analysis, a detailed inspection of the global graphical output provided by the `iacob-broad` tool (see Figs. 1 and 2) – including the observed and simulated line-profiles and their Fourier transforms – allows us to ascertain that the most critical cases found by Aerts et al. are not represented in the analyzed sample.

A representative example of results from the analysis of a star with a dominant macroturbulent broadening contribution is presented in Fig. 2, and we comment on this in Sect. 3.2. Figure 8 shows two examples of line profiles affected by non radial pulsations (β Cep stars in this specific case). Although the profiles are clearly asymmetric and have strong local jumps, their analysis does not offer a particular difficulty compared with similar stars that show smoother profiles (see e.g., Fig. 1).

In addition, the good agreement found between $v \sin i$(FT) and $v \sin i$(GOF,Θ_{RT}) from the analysis of our high-resolution, high S/N spectroscopic dataset suggests that for poor-quality spectroscopic datasets (e.g., fainter Galactic OB stars, or extragalactic objects) we can adopt the values derived from the GOF method, because it is less sensitive to noise than the FT method, whenever a radial-tangential formulation is adopted and a photospheric, unblended metal line is used for the analysis.

4.2. Macroturbulent broadening in Galactic OB stars

Figure 9 shows the $v \sin i$ and Θ_{RT} measurements of the whole sample plotted against spectral types for three different luminosity classes. Following Sect. 3.5.3, all Θ_{RT} measurements for stars with $v \sin i \geq$ 180 km s^{-1} have been marked as upper limits in the lower panels. We also indicate with gray zones the regions in which $v \sin i$ and Θ_{RT} measurements can be significantly affected

[5] A quantitative spectroscopic analysis aimed at determining the stellar and wind parameters of the whole IACOB sample is now in progress. Results will be presented in a forthcoming paper.

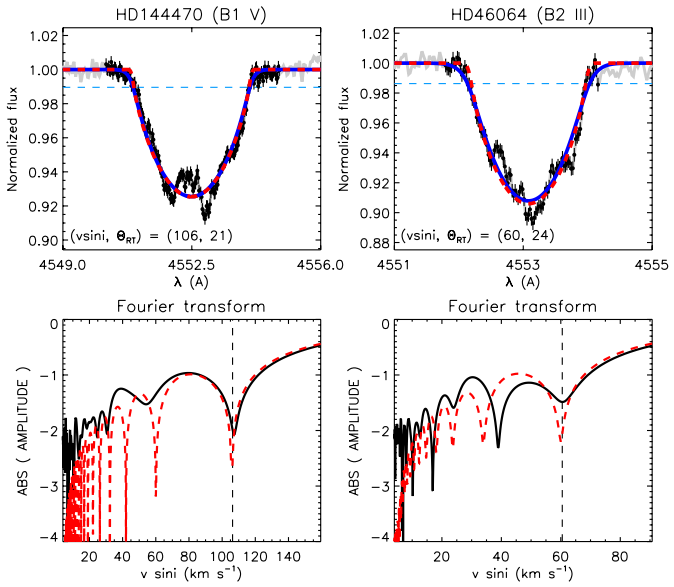

Fig. 8. Representative examples of the FT+GOF analysis for stars with features associated to β Cep-type non radial pulsations. The dashed red lines correspond to profiles with $v \sin i$(FT) and $\Theta_{RT} = 0$. The blue lines (only indicated in the *upper panels*) also include the additional broadening resulting from the GOF.

by the effect of microturbulence (see Sect. 3.4). In particular, we recall that within these regions, an Θ_{RT} measurement may be completely attributable to microturbulence, and any $v \sin i$ measurement must be considered as an upper limit.

At this point, the upper panels in Fig. 9 are only included for comparative purposes (in terms of range of measured values, trends, and dispersion) with the information provided in the lower panels. A more detailed discussion of the $v \sin i$ distributions (in a global sense and separated according to spectral types and luminosity classes) is presented in Sects. 4.3.2 and 4.3.3.

An important outcome from our study is the confirmation that the so-called macroturbulent broadening is present not only in B Sgs, but also in O-type stars of all luminosity classes (as the analysis of smaller samples have also begun to show, e.g. Bouret et al. 2012; Markova et al. 2014). This result has very important implications for our knowledge about the rotational properties of massive stars based on results from previous studies that used methods that do not properly separate rotation from macroturbulent broadening (see Sect. 4.3).

The strong correlations (with some dispersion) found between Θ_{RT} and spectral type are interesting as well, as is the observation that the size of the macroturbulent broadening seems to be slightly larger for supergiants than for giants and dwarfs with the same spectral type[6].

More information about the observational characteristics of the macroturbulent broadening (this time vs. $v \sin i$) is presented in Fig. 10. Results for the global sample are separated into three panels, from top to bottom: supergiants, (bright) giants, and dwarfs. O- and B-type stars are presented as filled and dotted circles, respectively. All Θ_{RT} measurements for stars with $v \sin i \geq 180$ km s^{-1} are indicated as upper limits. These are included for completeness, but are excluded from the discussion below. The regions where $v \sin i$ and Θ_{RT} measurements can be affected by microturbulence are also indicated. Dashed lines show the 1:1 relation. These lines roughly separate the regions where either rotational or macroturbulent broadening dominates.

We note the very different dependence of the macroturbulent broadening with $v \sin i$ for the three luminosity classes in O- and early-B type stars. While the distribution of stars in the Θ_{RT} vs. $v \sin i$ plane is very similar for O supergiants, giants, and dwarfs (with $v \sin i \leq 180$ km s^{-1}!), the relative number of early B-type stars in which macroturbulence dominates decreases from supergiants to dwarfs. In particular, we found no early-B dwarf in our sample with a dominant macroturbulent component and, conversely, all but two B Sgs are dominated by non rotational broadening. The two exceptions are HD 47240 and HD 191877, both classified as B1 Ib; the first one shows disk-like features in its spectrum (see also Lefever et al. 2007). We note that these two stars are also the only B Sgs in our sample with a projected rotational velocity higher than 100 km s^{-1}.

Figure 10 also shows a strong correlation between Θ_{RT} and $v \sin i$ in the region where macroturbulent broadening dominates. This correlation has also been pointed out by Markova et al. (2014) in a parallel work combining their own results and values from other authors in the literature. The correlation occurs for a range in the $\Theta_{RT}/v \sin i$ ratio between 1 and ~2.2 (the latter is marked with the dotted line). Interestingly, while the relative number of early B-type stars within this region diminishes when moving from luminosity class I to V, all O- and early-B stars with $\Theta_{RT} \geq v \sin i$ follow a similar behavior in terms of relative broadening.

This is not the case in the region below the 1:1 relation, where the line-broadening behavior of O- and early-B stars is very different. On the one hand, O-type stars mainly concentrate on a second sequence characterized by $\Theta_{RT}/v \sin i \sim 0.7$, which is independent of luminosity class. On the other hand, for early B giants and dwarfs (only two Sgs are found in this region), the macroturbulent broadening contribution is negligible (and probably attributable to microturbulence, see below) below $v \sin i \sim 80$–100 km s^{-1}, and seems to increase with $v \sin i$ above this value.

It is also interesting to look at the percentage of stars found within or close to the region where the measured Θ_{RT} can be interpreted as microturbulence (see also Fig. 9). All supergiants (except for one with $v \sin i \sim 200$) have Θ_{RT} values above the 40 km s^{-1} limit indicated in Sect. 3.4. In the case of (bright) giants there are a few early-B stars (but no O-type stars) close to the limit of 30 km s^{-1}. Interestingly, some of them correspond to non radial β Cep-type pulsators (the case illustrated in Fig. 8). Finally, the number of dwarfs with $v \sin i \leq 150$ km s^{-1} in which the measured Θ_{RT} can indeed be attributed to microturbulence is larger. These are mainly early-B and late-O dwarfs.

These results impose strong observational constraints to any theoretical attempt to provide an explanation for this line-broadening of still unconfirmed physical origin. While we here mainly concentrate on the impact of macroturbulent broadening on measurements of projected rotational velocities in Galactic OB stars, in a forthcoming paper (see Simón-Díaz et al. 2012, for some preliminary results) we will investigate whether the pulsational hypothesis proposed by Lucy (1976) and Aerts et al. (2009) fulfills the above mentioned observational requirements. We also refer to Markova et al. (2014), where some first steps toward understanding the observational characteristics of the additional line-broadening as a function of stellar parameters and evolution is presented.

[6] This second statement must be considered carefully, since our Θ_{RT} measurements include both the effect of macro- and of microturbulence (see notes in Sect. 3.4).

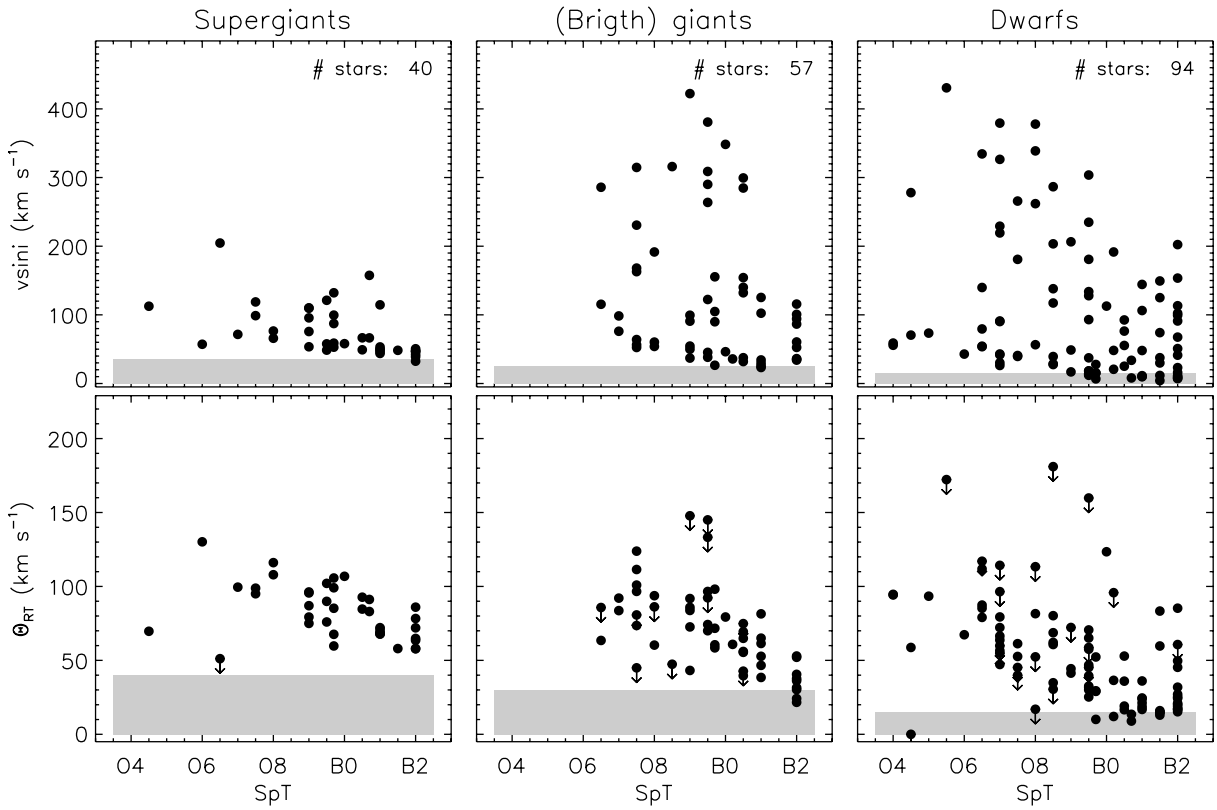

Fig. 9. $v \sin i$ and Θ_{RT} measurements vs. spectral types from the analyzed sample of OB-type stars. Θ_{RT} measurements for stars with $v \sin i \geq 180$ km s^{-1} can only be considered as upper limits (see text for explanation) and hence a downward arrow is added to the corresponding filled circles in the *lower panels*.

4.3. Projected rotational velocities in Galactic OB stars

4.3.1. Comparison with previous works: the effect of macroturbulent broadening

The main reference studies of rotational velocities in large samples of Galactic O- and early B-type stars are those by Slettebak (1956), Conti & Ebbets (1977, hereafter CE77), Penny (1996, hereafter P96), and Howarth et al. (1997, hereafter H97). All these studies based their $v \sin i$ measurements on methodologies that assume that the line profile is exclusively broadened by rotation. These and even earlier authors (viz. Struve 1952) already indicated, following indirect statistical arguments, that rotation was very likely not the only broadening agent of metal lines in early-type stars. They argued that the absence of very narrow line stars in their large samples could be explained by assuming some kind of additional line-broadening.

As stated in the introduction, the advent of high-resolution, very efficient spectrographs has allowed us to overcome the limitations imposed by observations in the first attempts of separating the various broadening contributions (e.g. Slettebak 1956), as well as to confirm their hypotheses. The analysis of these improved datasets definitely shows that $v \sin i$ measurements that do not account for the additional broadening overestimate the actual projected rotational velocities (see Simón-Díaz 2011, and references therein)

Comparisons with previous studies that did not consider macroturbulence can be found, among others, in Fraser et al. (2010), who presented a comparison of 42 B Sgs in common with with H97 (with spectral types ranging from B0 to B5), or in a study parallel to ours by Markova et al. (2014), who have compared their $v \sin i$(FT) results with those obtained by H97 for a small (but representative) sample of Galactic O-type stars. In this paper, we extend this investigation using a larger sample of Galactic O- and early-B type stars analyzed homogeneously.

For the sake of clarity, and taking into account that similar conclusions are expected to arise when considering the other studies, we concentrated our investigation on the comparison of our measurements with those derived by H97. These authors provided estimates for the $v_e \sin i$ linewidth parameter for 373 Galactic O-type and early B-Sgs obtained by means of applying a cross-correlation technique to high-dispersion IUE spectra. The derived quantities are hence representative of the projected rotational velocities that are derived when only rotation is taken into account (i.e., are similar to the cases of Slettebak, Conti et al.).

We have ~100 stars in common with them (namely ~80 O-type stars and ~20 early-B Sgs). Results from the comparison of the global sample are presented in Fig. 11. As expected, our estimates are systematically lower below $v \sin i \sim 100$ km s^{-1}. Globally, there is a systematic offset in this $v \sin i$ regime of ~25 km s^{-1}; however, differences of up to ~50 km s^{-1} can be found in some cases with intermediate projected rotational velocities. On the other hand, while there is a relatively good agreement above $v \sin i \sim 120$ km s^{-1}, the intermediate region presents a combined situation in which the additional broadening still affects the $v \sin i$ measurements in some cases (mainly O stars, see below). The impact on the global $v \sin i$ distribution is clear: the peak of the distribution is shifted downward from ~90 km s^{-1} to ~50 km s^{-1}, and the number of cases with $v \sin i$ below 40 km s^{-1} is multiplied by a factor 2.

Comparison of results for the O stars and B Sgs samples is presented separately in Figs. 12 and 13, respectively. Once more,

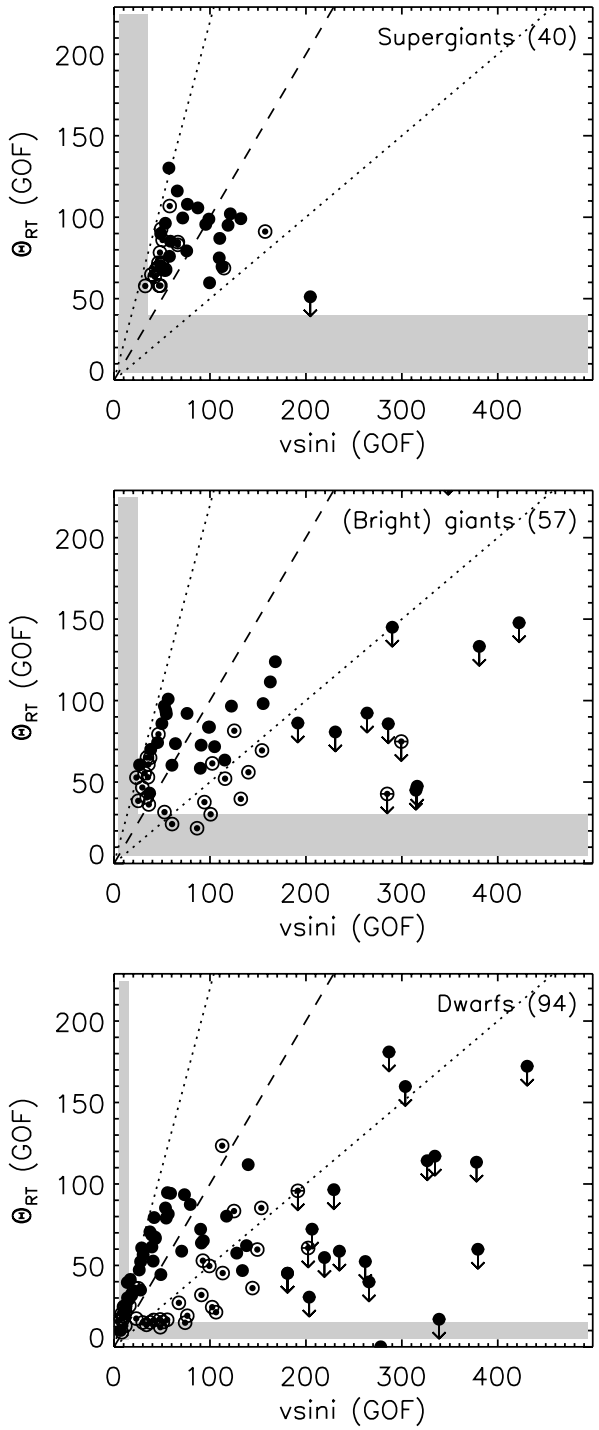

Fig. 10. Θ_{RT} vs. $v \sin i$ for the stars in where $v \sin i$(FT) and $v \sin i$(GOF) agree to better than 20%. Filled and dotted circles indicate the O- and B-type stars, respectively. The indicated values of Θ_{RT} for all the stars with $v \sin i \geq 180$ km s^{-1} must be considered as upper limits. The regions in which $v \sin i$ and Θ_{RT} measurements can be affected by the effect of microturbulent broadening (see text for explanation) are indicated in gray. Dashed and dotted lines indicate the 1:1, 2.2:1, and 1:0.5 relations, respectively.

the effect of the non rotational broadening on $v \sin i$ determinations is shown to be significant not only in B Sgs, but also in O stars of all luminosity classes. Even O dwarfs with low $v \sin i$ are affected.

For the sake of completeness, we note here that the statement about the downward revision of previous $v \sin i$ determinations is not applicable for early-B dwarfs. As shown in Fig. 10, the macroturbulent contribution to the line-profile is negligible compared with that of the rotational broadening and hence a very good agreement between $v \sin i$(FT) and measurements that do not account for macroturbulent broadening is expected.

4.3.2. New $v \sin i$ distributions

Figure 14 groups the histograms resulting from the analysis of the global IACOB sample separated by spectral type (rows) and luminosity class (columns). The row at the top includes all the O-type stars, while the bottom row corresponds to the early B-type stars. Panels in between show the distributions for the O stars separated into early, mid, and late spectral types, respectively.

Before we comment on this figure we note that the histogram corresponding to the early-B dwarfs has only been included for completeness, but must be left out from any discussion about $v \sin i$ distributions since at present the IACOB spectroscopic database is totally biased toward (relatively) narrow-line stars for these specific stars[7]. For a more complete overview of the distribution of projected rotational velocities in B-type stars in the Milky Way we refer for instance to Abt et al. (2002), Strom et al. (2005), Huang & Gies (2006, 2008), Wolff et al. (2007), Huang et al. (2010), and Bragança et al. (2012). In all these works it was shown that the distribution of projected rotational velocities of early-B dwarfs extends farther, to $v \sin i$ values higher than 200 km s^{-1}.

The number of stars in some of the histograms is not large enough to extract conclusions with the desired statistical significance; however, we can highlight some trends (many of them in concurrence with previous studies by CE77, P96, and H97). As stated in previous works, the global sample of Galactic O stars presents a bimodal distribution, containing a slow group with a $v \sin i$ peak near 40–60 km s^{-1} and a fast group extending up to ~400 km s^{-1}. Interestingly, the low $v \sin i$ peak has now been revised downward with respect to the 80–100 km s^{-1} indicated by CE77, P96, and H97. This is basically an effect of the separation of the macroturbulent contribution from the total broadening (see Sect. 4.3.1).

This bimodal distribution has recently also been obtained by Ramírez-Agudelo et al. (2013) in their study of rotational velocities in the O-star population of the 30 Doradus region. A similar analysis of 216 apparently single O-type stars in this star-forming region of the Large Magellanic Cloud led to a low $v \sin i$ peak located at 40–80 km s^{-1}, and the high $v \sin i$ tail extending up to ~600 km s^{-1}. In the case of stars in 30 Dor, the high $v \sin i$ tail extends farther toward higher rotation speeds, as expected from the lower metal content of the region ($Z_{30Dor} \sim 0.5\ Z_{\odot}$). Unfortunately, the accuracy of $v \sin i$ measurements in the study by Ramírez-Agudelo et al. does not allow one to firmly conclude whether there is any difference in the location of the peak distribution.

Conti & Ebbets (1977) indicated at the time that we were somewhat at a loss to understand the apparent existence of a bimodal distribution for the main sequence O stars. Today, we can count on an interesting scenario to explain this result (de Mink et al. 2013). In brief, de Mink et al. proposed that the observed

[7] The early-B dwarfs in the IACOB spectroscopic database mainly come from the study of abundances in B-type stars in Orion OB1 (Simón-Díaz 2010; Nieva & Simón-Díaz 2011) and the construction of an atlas of standard stars for spectral classification at intermediate and high resolution.

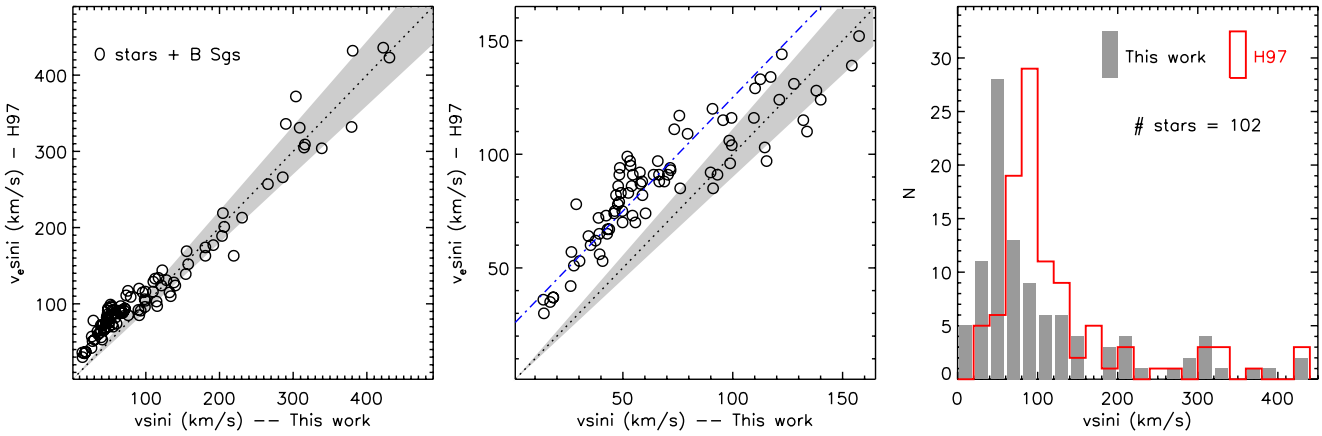

Fig. 11. Comparison with H97 (all stars in common). *Left panel*: $v_e \sin i$ (H97) vs. $v \sin i$(GOF); the one-to-one relation is indicated with a dotted line and the <10% difference region in gray. *Center panel*: same as before, but zoomed-in on the region below 150 km s^{-1} (the dash-dotted line corresponds to $v \sin i$(GOF) + 28 km s^{-1}). *Right*: comparison of the corresponding histograms (bin size =20 km s^{-1}) resulting from both studies.

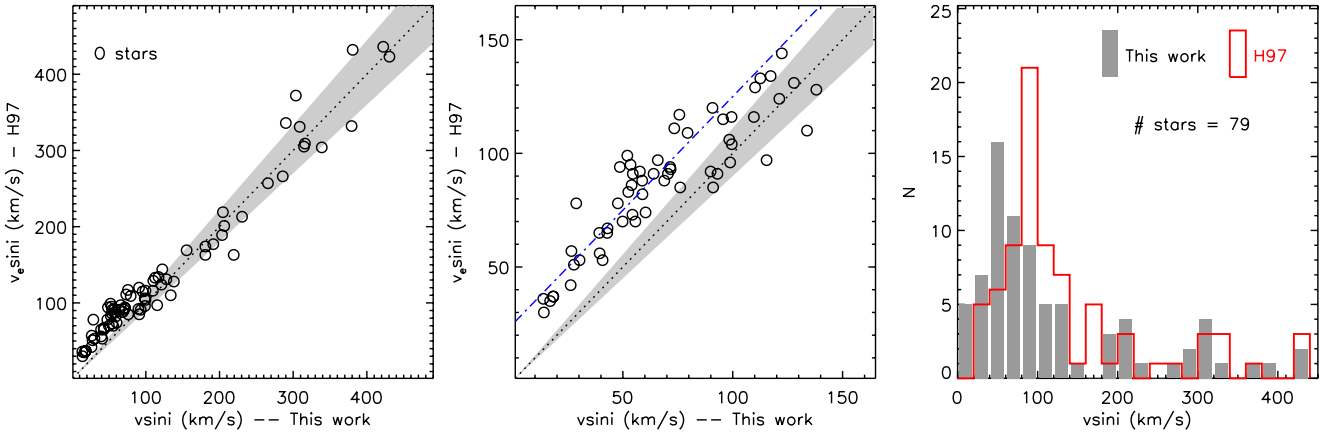

Fig. 12. Comparison with H97 (O stars in common). See Fig. 11 for explanations of the various panels.

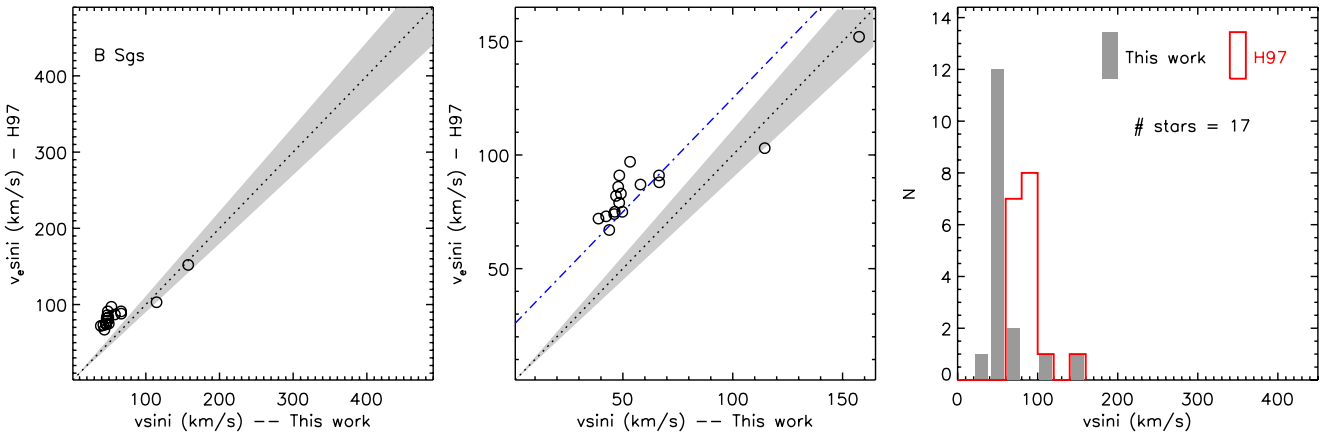

Fig. 13. Comparison with H97 (B Sgs in common). See Fig. 11 for explanations of the various panels.

distribution may be a consequence of the combined effect of stellar winds, expansion, tides, mass trasfer, and mergers. In particular, the high $v \sin i$ tail supposedly mainly contains products resulting from massive-star binary interaction. For the purpose of comparison with the predictions by de Mink et al. (or a new proposed scenario), we indicate in Table 1 the number and percentage of stars in various $v \sin i$ ranges of interest. The good agreement between the predictions by de Mink et al., who assumed a constant star formation rate, and our percentages of observed O stars with $v \sin i > 200$ and 300 km s^{-1} (23% and 11%, respectively) agree remarkably well. We also note that these percentages are almost equal to those resulting from the studies by CE77, P96, and H97. This is because above ~120 km s^{-1} the effect of the macroturbulent contribution to the global broadening is practically negligible when compared to rotational broadening (see Sect. 4.3.1).

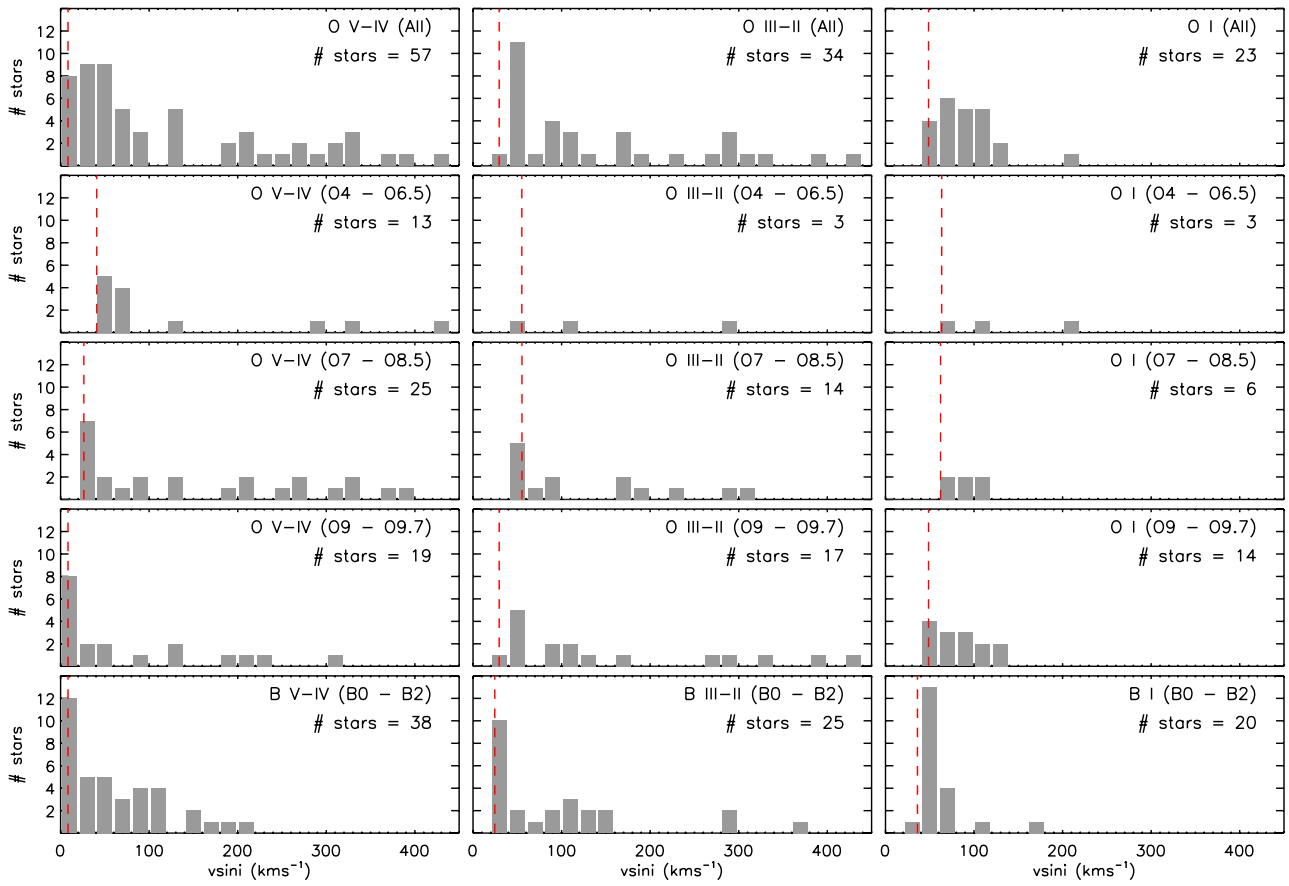

Fig. 14. Histograms resulting from the complete analyzed sample. *From left to right*: dwarfs, (bright) giants, and supergiants. *From top to bottom*: all O stars, early-O, mid-O, late-O, and all early-B stars with a given luminosity class. Vertical dashed lines indicate the minimum $v \sin i$ measured in the specific sample (see also Fig. 15).

Table 1. Number of stars for various $v \sin i$ ranges of interest (see text).

SpT & LC	$v \sin i$ [km s^{-1}]				
All LC	<50	<200	>200	>300	All
O stars	31 (26%)	90 (77%)	26 (22%)	12 (10%)	116
Early B Sgs	10 (50%)	20 (100%)	0 (0%)	0 (0%)	20
(V – IV)	<50	<200	>200	>300	All
All O	24 (42%)	41 (71%)	16 (28%)	8 (14%)	57
Early O	3	10	3	2	13
Mid O	9	15	10	5	25
Late O	12	16	3	1	19
(III – II)	<50	<200	>200	>300	All
All O	4 (11%)	25 (73%)	9 (26%)	4 (11%)	34
Early O	0	2	1	0	3
Mid O	0	11	3	1	14
Late O	4	12	5	3	17
(I)	<50	<200	>200	>300	All
All O	1 (4%)	22 (95%)	1 (4%)	0 (0%)	23
Early O	0	2	1	0	3
Mid O	0	6	0	0	6
Late O	1	14	0	0	14

Notes. The ranges in SpT correspond to those indicated in Figs. 14 and 15.

If we now split the distribution of projected rotational velocities in spectral type and luminosity class it can be concluded that the high velocity tail completely disappear in the case of O Sgs (see also Table 1), where stars concentrate at $v \sin i$ = 40–140 km s^{-1}. Interestingly, the distribution of B Sgs (which are considered the evolved stages of the mid and early O-type stars) also present a single peak distribution concentrated in the low $v \sin i$ regime. This result was already pointed out by H97; the only difference found here is that while H97 found the peaks of the two distributions at ~90 and 70 km s^{-1} (O and

B Sgs, respectively), our results led to 70 km s^{-1}, and 50 km s^{-1}, respectively.

Another result that has attracted our attention concerns the comparison of the $v \sin i$ distributions corresponding to the evolutionary sequence starting in the mid-O dwarfs and ending in the early-B Sgs (i.e., the diagonal from the O7 – O8.5 V – IV panel to the B0 – B2 I panel). Independently of the origin of the high $v \sin i$ tail, the (almost) absence of early-B Sgs with projected rotational velocities higher than 100 km s^{-1} can be used as observational evidence that evolution causes fast rotators to spin down very efficiently. However, if the same mechanisms that causes these stars to slow down affect all mid-O dwarfs, we would expect a larger number of early-B Sgs with lower $v \sin i$. In fact, the peak of the distribution of early-B Sgs is located at somewhat higher $v \sin i$ values than that corresponding to the mid-O dwarfs. This result, also indicated by Howarth (2004) in a more general context, was used by previous authors as an indirect proof of the presence of some non rotational macroscopic line-broadening operating in massive stars. However, the techniques applied here are assumed to provide actual projected rotational velocities. Therefore, either there is something that we still do not understand from an evolutionary point of view (E.g., is the mechanism that reduces the surface rotation of massive stars different for fast rotators and intermediate and low $v \sin i$ stars?), or our efforts to separate rotation from other sources of line-broadening are still failing in some cases.

In the next section we discuss in more detail this (and other) remaining questions regarding the low $v \sin i$ region of the distributions and also provide a possible explanation and some guidelines for future investigations.

4.3.3. Low $v \sin i$ regime

The long-standing problem of the small number of low $v \sin i$ O-type stars and early-B Sgs (CE77, P96, H97) seems now to be partially solved in view of the diagrams presented in Figs. 11–13. In particular, in Sect. 4.3.2, we pointed out when comparing with previous results by H97 that the number of O stars with measured $v \sin i$ values below 40 km s^{-1} is now multiplied by a factor 2. However, from closer inspection of the $v \sin i$ distributions separated by spectral type and luminosity class (Fig. 14), one might conclude that despite this improvement, there still seems to be some limitation in the detectability of the very low $v \sin i$ stars. In addition to the evolutionary considerations indicated at the end of previous section, looking at Fig. 15, where we show the minimum detected $v \sin i$ in different spectral type boxes and taking into account statistical arguments based on the probability to find stars with a given inclination angle, it is remarkable that

- no O Sgs with $v \sin i < 50$ km s^{-1} are found[8]. The situation is even more critical for the case of mid- and early-O Sgs, where the lower $v \sin i$ measured is ~60 km s^{-1}. We note, however, the very low statistics in this latter case (only seven stars have been analyzed).
- While the relative number of B0 – B2 Sgs with measured projected rotational velocities below 50 km s^{-1} is considerably larger (~50%), the FT+GOF analysis does not result in a $v \sin i < 35$ km s^{-1} for any of them, and only 2 of a total of 20 have a $v \sin i < 40$ km s^{-1}.
- There is no problem with the relative number of low $v \sin i$ stars found in the case of early-B and late-O dwarfs. There is a fair number of O9 – B2 dwarfs in the IACOB sample with measured $v \sin i$ below 40 km s^{-1}, and the lower $v \sin i$ measured for this category is of about 10 km s^{-1}.
- But for mid- and early-O dwarfs there still seems to be a limit in the minimum detected $v \sin i$. This limit increases from ~25 km s^{-1} for mid-O dwarfs to ~40 km s^{-1} for the dwarfs with spectral types earlier than O6.5.
- A similar situation occurs for the O stars with luminosity classes III and II (this time also including the late O spectral types). Again, the lower limit in the measured $v \sin i$ increases from ~30 km s^{-1} to ~55 km s^{-1} from the latest to the earliest spectral types.
- Finally, a low $v \sin i$ limit of ~ 25 km s^{-1} is also found in the early-B (bright) giants.

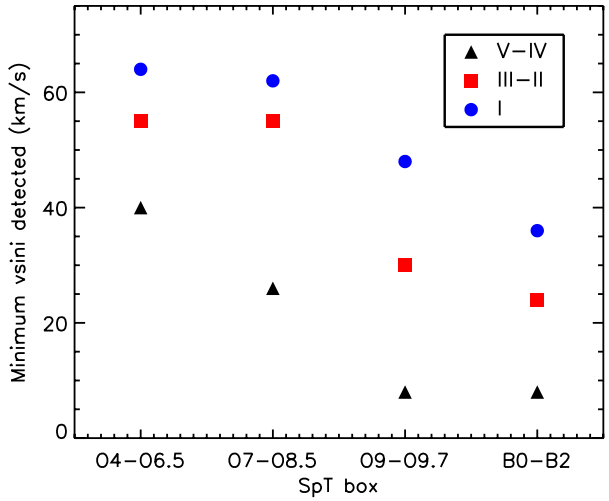

Fig. 15. Minimum $v \sin i$ measured for specific sub-samples, separated by SpT and LC. The indicated values correspond to the dashed vertical lines in Fig. 14.

One possible explanation of this dependence of the minimum detected $v \sin i$ on spectral type and luminosity class is related to the effect of microturbulence on $v \sin i$ measurements. As indicated in Sect. 3.4, microturbulence can impose a lower detectability limit on the actual projected rotational velocity when a strategy similar to the one considered in our study is applied. The rough estimates obtained from the exercise presented in Sect. 3.4 indicate that for a star with a microturbulence of 20 km s^{-1}, a $v \sin i \leq 35$ km s^{-1}should be actually considered as an upper limit. Since microturbulent velocities ~15–20 km s^{-1}are typically found for early-B Sgs, this may explain why no B Sgs with $v \sin i \leq 40$ km s^{-1} are found. On the other hand, microturbulent velocities in the range 1–7 km s^{-1} and 10–15 km s^{-1} (Rough numbers!) are derived for B dwarfs and giants, respectively. This would make the effect of microturbulence not as critical for B dwarfs (as indicated in Sect. 3.4 if microturbulence is 5 km s^{-1} the upper $v \sin i$ limit moves down to ~10 km s^{-1}), and intermediate for B giants.

What is the situation for mid- and early O-type stars? Unfortunately, a direct estimation of microturbulent velocities from the analysis of observed spectra of mid- and early O-type stars is not as straightforward as in the case of B-type and late O-type stars. Extrapolating the trends of microturbulence observed for B-type stars (where it was found that microturbulent velocities are a factor 2–3 higher in early-B than in late-B Sgs) to the O-type stars domain could explain the tendency observed in Fig. 15. However, this is by far too risky and, in addition, the associated microturbulent velocities expected for the earliest spectral types would be too high.

[8] There is one star (HD 37742), but is has $v \sin i = 48$ km s^{-1}.

One could also consider the predictions by Cantiello et al. (2009). These authors proposed that a physical connection might exist between microturbulence in hot star atmospheres and subphotospheric convective motions associated to the iron convection zone. Under this hypothesis, they predicted the regions in the HR diagram where higher values of microturbulent velocities should be expected. Interestingly, while the predictions for the late-O/early-B star domain roughly follow the observed tendency, values of microturbulence predicted for early- and mid-O-dwarfs are not expected to be particularly large compared to later spectral types.

5. Summary and future prospects

We reassessed previous determinations of projected rotational velocities ($v \sin i$) in Galactic OB stars using a large, high-quality spectroscopic dataset (drawn from the IACOB spectroscopic database of northern Galactic OB stars) and a powerful technique that accounts for other sources of line-broadening in addition to the rotation. In particular, we investigated the effect of macroturbulent and microturbulent broadenings on $v \sin i$ measurements.

Motivated by the investigation presented here we developed a versatile and user-friendly IDL tool – based on a combined Fourier transform (FT) + goodness-of-fit (GOF) methodology – for the line-broadening characterization in OB-type stars: the `iacob-broad`. The procedure allows one to extract information about $v \sin i$ and the macroturbulent broadening ($v_{\rm m}$) from the stellar line-profiles under a variety of situations. The `iacob-broad` was used for three purposes:

1. To investigate the effect that the assumed macroturbulent profile (either isotropic Gaussian or radial-tangential) has on $v \sin i$ and $v_{\rm m}$ estimations based on the GOF.
2. To investigate the possible consequences of neglecting the effect of microturbulence on the determination of these two quantities.
3. To determine $v \sin i$ and the size of the macroturbulent broadening in a sample of ∼200 Galactic OB-type stars with spectral types ranging from O4 to B2 and covering all luminosity classes. In particular, we compared the derived $v \sin i$ with previous determinations that did not account for the macroturbulent broadening contribution.

We showed that $v \sin i$ and $v_{\rm m}$ determined by means of the GOF method critically depend on the assumed macroturbulent profile, and presented further observational evidence supporting a previous statement quoted in Simón-Díaz et al. (2010), which indicated that a radial-tangential description is better suited to infer GOF-based projected rotational velocities. While the derived $v \sin i$(GOF,$\Theta_{\rm RT}$) values agreed perfectly with those resulting from the FT analysis, the isotropic Gaussian profile systematically led to much lower values of $v \sin i$.

The very good agreement found between $v \sin i$(FT) and $v \sin i$(GOF, $\Theta_{\rm RT}$) from the analysis of our high-resolution, high S/N spectroscopic dataset suggests that for poor-quality datasets (e.g. fainter Galactic OB stars, or extragalactic objects) we can adopt the values provided by the GOF method, because it is less sensitive to noise than the FT method, whenever a radial-tangential formulation of the macroturbulent profile is adopted.

We also cautioned about the danger of combining measurements of the macroturbulent velocity provided by different authors in the literature when they were obtained by assuming a different macroturbulent profile.

Following the guidelines by Gray (1976), we showed that any $v \sin i$ and $\Theta_{\rm RT}$ measurement in OB-type stars (either from FT of GOF) below ∼40 km s^{-1} must be considered as an upper limit if the effects of microturbulence are not taken into account in the line-broadening analysis.

An important result from our study is the confirmation that the macroturbulent broadening is present not only in B Sgs, but also in O-type stars of all luminosity classes (as the analysis of smaller samples had previously begun to show). As a consequence, previous determinations of $v \sin i$ not accounting for the additional broadening need to be systematically revised downward[9] in these types of stars by 25 (±20) km s^{-1} when the derived $v \sin i$ was below ∼120 km s^{-1}. This implies important modifications of the distributions of projected rotational velocities in Galactic OB-type stars. In particular, the low $v \sin i$ peak previously found in 80–100 km s^{-1} (in the global $v \sin i$ distributions) has now been revised downward to 40–60 km s^{-1}.

Although the long-standing problem of the small number of low $v \sin i$ O-type stars and early-B Sgs has now partially been solved, there still seems to remain some limitation in the detectability of the very low $v \sin i$ stars, particularly for mid- and early-O stars and the early-B Sgs. We found some interesting trends of the minimum detected $v \sin i$ in our analyzed sample of Galactic stars with spectral type and luminosity class. We indicated that this result might be an effect of the limitations of the FT+GOF strategy when microturbulence is not taken into account.

It is still too early to conclude that the effect of microturbulence on $v \sin i$ measurements is the cause of this observational result; however, this is an interesting possibility that should be explored in more detail in the future. As a guide we proposed three different aspects to be investigated. From a methodological point of view, is it possible to separate the spectroscopic features (either in the wavelength or the Fourier domains) associated to microturbulence from those exclusively produced by rotation? From an observational point of view, can we increase our knowledge about the microturbulence in O-type stars? And, from a theoretical/modeling point of view, explore further the scenario proposed by Cantiello et al. (2009) and compare the corresponding predictions with observational constraints.

In addition, the extension of this type of study to other metallicities (also increasing the number of analyzed stars in the Galaxy with the incorporation of the Southern sample), and the exploration of other possible effects that may invalidate our state-of-the-art techniques used to measure projected rotational velocities in O- and B-type stars (under certain circumstances) are also warranted.

Acknowledgements. This work has been funded by the Spanish Ministry of Economy and Competitiveness (MINECO) under grants AYA2010-21697-C05-04, Consolider-Ingenio 2010 CSD2006-00070, and Severo Ochoa SEV-2011-0187, and by the Canary Islands Government under grant PID2010119. SS-D kindly acknowledges the staff at the Nordic Optical Telescope for their professional competence and always useful help during more than 50 observing nights between 2008 and 2013. SS-D also thanks his observing colleagues I. Negueruela, J. Lorenzo, N. Castro and M. Garcia. We are extremely grateful to N. Langer and the referee, F. Royer, for the time devoted to read the first version of the paper and his very useful and constructive comments.

References

Abt, H. A., Levato, H., & Grosso, M. 2002, ApJ, 573, 359
Aerts, C., Puls, J., Godart, M., & Dupret, M.-A. 2009, A&A, 508, 409
Aerts, C., Simón-Díaz, S., Catala, C., et al. 2013, A&A, 557, A114

[9] This statement is not applicable to early-B dwarfs, where the macroturbulent broadening contribution to the line profiles is negligible.

Bouret, J.-C., Hillier, D. J., Lanz, T., & Fullerton, A. W. 2012, A&A, 544, A67
Bouret, J.-C., Lanz, T., Martins, F., et al. 2013, A&A, 555, A1
Bragança, G. A., Daflon, S., Cunha, K., et al. 2012, AJ, 144, 130
Cantiello, M., Langer, N., Brott, I., et al. 2009, A&A, 499, 279
Carroll, J. A. 1933, MNRAS, 93, 478
Conti, P. S., & Ebbets, D. 1977, ApJ, 213, 438
de Mink, S. E., Langer, N., Izzard, R. G., Sana, H., & de Koter, A. 2013, ApJ, 764, 166
Degroote, P., Briquet, M., Auvergne, M., et al. 2010, A&A, 519, A38
Dufton, P. L., Ryans, R. S. I., Simón-Díaz, S., Trundle, C., & Lennon, D. J. 2006, A&A, 451, 603
Dufton, P. L., Langer, N., Dunstall, P. R., et al. 2013, A&A, 550, A109
Ebbets, D. 1979, ApJ, 227, 510
Fraser, M., Dufton, P. L., Hunter, I., & Ryans, R. S. I. 2010, MNRAS, 404, 1306
Frémat, Y., Zorec, J., Hubert, A.-M., & Floquet, M. 2005, A&A, 440, 305
Georgy, C., Meynet, G., Walder, R., Folini, D., & Maeder, A. 2009, A&A, 502, 611
Gray, D. F. 1973, ApJ, 184, 461
Gray, D. F. 1976, The observation and analysis of stellar photospheres Research supported by the National Research Council of Canada (New York: Wiley-Interscience)
Gray, D. F. 2005, The Observation and Analysis of Stellar Photospheres, 3rd edn. (Cambridge University Press)
Grunhut, J. H., Wade, G. A., Sundqvist, J. O., et al. 2012, MNRAS, 426, 2208
Howarth, I. D. 2004, Stellar Rotation, 215, 33
Howarth, I. D., Siebert, K. W., Hussain, G. A. J., & Prinja, R. K. 1997, MNRAS, 284, 265
Huang, W., & Gies, D. R. 2006, ApJ, 648, 580
Huang, W., & Gies, D. R. 2008, ApJ, 683, 1045
Huang, W., Gies, D. R., & McSwain, M. V. 2010, ApJ, 722, 605
Hunter, I., Lennon, D. J., Dufton, P. L., et al. 2008, A&A, 479, 541
Hunter, I., Brott, I., Langer, N., et al. 2009, A&A, 496, 841
Langer, N. 2012, ARA&A, 50, 107
Lefever, K., Puls, J., & Aerts, C. 2007, A&A, 463, 1093
Lefever, K., Puls, J., Morel, T., et al. 2010, A&A, 515, A74
Lucy, L. B. 1976, ApJ, 206, 499
Maeder, A. 1987, A&A, 178, 159
Maeder, A., & Meynet, G. 2000, ARA&A, 38, 143
Markova, N., & Puls, J. 2008, A&A, 478, 823
Markova, N., Puls, J., Simón-Díaz, S., et al. 2014, A&A, 562, A37
Nieva, M.-F., & Simón-Díaz, S. 2011, A&A, 532, A2
Penny, L. R. 1996, ApJ, 463, 737
Przybilla, N., Firnstein, M., Nieva, M. F., Meynet, G., & Maeder, A. 2010, A&A, 517, A38
Puls, J., Urbaneja, M. A., Venero, R., et al. 2005, A&A, 435, 669
Ramírez-Agudelo, O. H., Simón-Díaz, S., Sana, H., et al. 2013, A&A, 560, A29
Ryans, R. S. I., Dufton, P. L., Rolleston, W. R. J., et al. 2002, MNRAS, 336, 577
Sana, H., de Mink, S. E., de Koter, A., et al. 2012, Science, 337, 444
Santolaya-Rey, A. E., Puls, J., & Herrero, A. 1997, A&A, 323, 488
Simón-Díaz, S. 2010, A&A, 510, A22
Simón-Díaz, S. 2011, Bull. Soc. Roy. Sci. Liège, 80, 86
Simón-Díaz, S., & Herrero, A. 2007, A&A, 468, 1063
Simón-Díaz, S., Herrero, A., Uytterhoeven, K., et al. 2010, ApJ, 720, L174
Simón-Díaz, S., Castro, N., Garcia, M., Herrero, A., & Markova, N. 2011a, Bull. Soc. Roy. Sci. Liège, 80, 514
Simón-Díaz, S., Garcia, M., Herrero, A., Maíz Apellániz, J., & Negueruela, I. 2011b, Stellar Clusters and Associations: Proc. A RIA Workshop on Gaia, eds. E. J. Alfaro Navarro, A. T. Gallego Calvente, & M. R. Zapatero Osorio, 255
Simón-Díaz, S., Castro, N., Herrero, A., et al. 2012, Proc. of a Scientific Meeting in Honor of Anthony F. J. Moffat, ASP Conf. Ser., 465, 19
Slettebak, A. 1956, ApJ, 124, 173
Smith, M. A., & Gray, D. F. 1976, PASP, 88, 809
Sota, A., Maíz Apellániz, J., Walborn, N. R., et al. 2011, ApJS, 193, 24
Strom, S. E., Wolff, S. C., & Dror, D. H. A. 2005, AJ, 129, 809
Struve, O. 1952, PASP, 64, 117
Sundqvist, J. O., Simón-Díaz, S., Puls, J., & Markova, N. 2013, A&A, 559, L10
Townsend, R. H. D., Owocki, S. P., & Howarth, I. D. 2004, MNRAS, 350, 189
Wilson, A. 1969, MNRAS, 144, 325
Wolff, S. C., Strom, S. E., Dror, D., & Venn, K. 2007, AJ, 133, 1092

Pages 18 to 22 are available in the electronic edition of the journal at http://www.aanda.org

Appendix A: Tables

Table A.1. Results from the `iacob-broad` analysis of the O- and B Supergiants (LC I).

HD number	SpT	LC	Line	EW [mÅ]	S/N	$v \sin i$(FT) [km s^{-1}]	$v \sin i$(GOF) [km s^{-1}]	$v_{\rm m}$(GOF) [km s^{-1}]
HD 14947	O4.5	If	OIII	90	250	107	112	69
HD 169582	O6	Iaf	OIII	196	218	63	57	130
HD 210839	O6.5	I(n)fp	OIII	231	380	204	204	51
HD 193514	O7	Ib(f)	OIII	306	172	62	71	99
HD 188001	O7.5	Iabf	OIII	344	255	89	71	112
HD 192639	O7.5	Iabf	OIII	349	272	104	98	98
HD 17603	O7.5	Ib(f)	OIII	295	226	118	118	95
HD 225160	O8	Iabf	OIII	262	249	89	76	107
HD 167971	O8	Ia(n)	OIII	374	213	62	65	116
HD 210809	O9	Iab	OIII	251	234	72	75	79
HD 202124	O9	Iab	OIII	263	232	95	95	95
HD 30614	O9	Ia	OIII	308	321	115	110	86
HD 209975	O9	Ib	OIII	264	319	53	53	96
HD 61347	O9	Ib	OIII	259	201	115	109	75
HD 188209	O9.5	Iab	OIII	201	271	60	57	75
HD 218915	O9.5	Iab	OIII	196	210	48	48	89
HD 37742	O9.5	IbNwkvar	OIII	249	390	127	121	102
HD 194280	OC9.7	Iab	OIII	159	250	91	87	105
HD 195592	O9.7	Ia	OIII	147	221	58	52	67
HD 47432	O9.7	Ib	OIII	145	284	99	99	59
HD 225146	O9.7	Iab	OIII	89	173	69	55	76
HD 18409	O9.7	Ib	OIII	197	261	132	132	99
HD 37128	B0	Ia	SiIII	321	437	60	48	111
HD 204172	B0	Ib	SiIII	271	258	61	58	106
HD 38771	B0.5	Ia	SiIII	357	267	54	49	92
HD 213087	B0.5	Ibe	SiIII	373	168	60	66	84
HD 2905	BC0.7	Ia	SiIII	446	259	66	66	83
HD 13854	B1	Iab	SiIII	455	179	48	53	67
HD 91316	B1	IabNstr	SiIII	425	370	49	49	72
HD 169454	B1	Ia+	SiIII	527	159	54	49	71
HD 47240	B1	Ib	SiIII	436	204	114	114	68
HD 191877	B0.7	Ib	SiIII	467	193	165	157	91
HD 24398	B1	Ib	SiIII	425	287	43	43	67
HD 119608	B1	Ib	SiIII	484	279	46	46	69
HD 190603	B1.5	Ia+	SiIII	512	229	48	48	57
HD 14818	B2	Ia	SiIII	420	204	44	46	58
HD 41117	B2	Ia	SiIII	457	239	43	38	64
HD 14956	B2	Ia	SiIII	508	151	50	50	85
HD 13841	B2	Ib	SiIII	445	89	51	46	72
HD 13866	B2	Ib	SiIII	368	161	43	47	78
HD 206165	B2	Ib	SiIII	348	253	42	42	63
HD 14443	BC2	Ib	SiIII	339	105	36	32	57

Table A.2. Results from the `iacob-broad` analysis of the O- and B (bright) giants (LCs II and III).

HD number	SpT	LC	Line	EW [mÅ]	S/N	$v \sin i$(FT) [km s^{-1}]	$v \sin i$(GOF) [km s^{-1}]	$v_{\rm m}$(GOF) [km s^{-1}]
HD 157857	O6.5	II(f)	OIII	217	210	115	115	63
HD 190864	O6.5	III(f)	OIII	269	307	55	68	82
HD 175876	O6.5	III(n)(f)	OIII	340	264	285	285	85
HD 171589	O7	II(f)	OIII	253	249	98	98	83
HD 167659	O7	II-III(f)	OIII	263	252	80	76	92
HD 34656	O7.5	II(f)	OIII	222	221	63	63	73
HD 35633	O7.5	II(n)(f)	OIII	398	288	176	168	123
HD 186980	O7.5	III((f))	OIII	336	256	55	52	96
HD 163800	O7.5	III	OIII	377	221	59	56	100
HD 203064	O7.5	IIIn((f))	OIII	281	280	299	314	44
HD 24912	O7.5	III(n)((f)	OIII	288	360	230	230	80
BD +60261	O7.5	III(n)((f)	OIII	310	217	171	162	111
HD 162978	O8	II	OIII	233	224	56	53	93
HD 175754	O8	II(n)(f)p	OIII	330	242	191	191	86
HD 36861	O8	III((f))	OIII	301	292	57	60	60
HD 218195A	O8.5	III	OIII	248	264	56	44	78
HD 13268	ON8.5	IIIn	OIII	197	256	315	315	47
HD 207198	O9	II	OIII	317	305	57	54	91
HD 24431	O9	III	OIII	254	307	55	49	85
HD 191423	ON9	II-IInn	OIII	225	218	422	422	147
HD 16832	O9.5	II-III	OIII	215	229	41	45	74
HD 166546	O9.5	II-III	OIII	179	340	42	38	70
HD 15137	O9.5	II-IIIn	OIII	223	237	290	290	145
HD 15642	O9.5	II-IIIn	OIII	214	186	325	308	243
HD 52266	O9.5	IIIn	OIII	135	193	263	263	92
HD 13022	O9.7	II-III	OIII	131	217	110	104	71
HD 55879	O9.7	III	OIII	121	326	29	26	60
HD 13745	O9.7	II(n)	OIII	160	216	163	155	98
HD 189957	O9.7	III	OIII	156	292	89	89	58
HD 48434	B0	III	SiIII	276	174	44	46	79
HD 165174	B0	IIIn	SiIII	327	205	366	348	238
HD 40111	B0.5	II	SiIII	365	193	140	140	56
HD 187459	B0.5	III	SiIII	408	188	154	154	69
HD 188439	B0.5	IIIn	SiIII	462	181	299	299	74
HD 218376	B0.5	III	SiIII	334	263	33	31	55
HD 184915	B0.5	IIIn	SiIII	471	242	284	284	42
HD 14052	B1	Ib-II	SiIII	355	102	36	34	65
HD 50707	B1	III	SiIII	273	228	24	29	46
HD 54764	B1	II	SiIII	456	202	125	125	81
HD 205139	B0.5	II-III	SiIII	340	226	34	37	64
HD 44743	B1	II/III	SiIII	307	238	26	25	38
HD 187879	B1	III	SiIII	361	233	102	102	61
HD 147165	B1	III	SiIII	260	246	24	23	52
HD 62747	B2	II	SiIII	252	243	100	100	30
HD 60325	B2	II	SiIII	245	204	115	115	52
HD 35468	B2	III	SiIII	201	324	52	52	31
HD 30836	B2	III	SiIII	247	199	38	36	36
HD 46064	B2	III	SiIII	124	218	60	60	24
HD 52273	B2	III	SiIII	204	236	86	86	21
HD 188252	B2	III	SiIII	243	237	94	94	37
HD 31327	B2	II	SiIII	313	183	35	35	52

Table A.3. Results from the `iacob-broad` analysis of the O dwarfs and subgiants (LC V and IV).

HD number	SpT	LC	Line	EW [mÅ]	S/N	$v \sin i$(FT) [km s^{-1}]	$v \sin i$(GOF) [km s^{-1}]	$v_{\rm m}$(GOF) [km s^{-1}]
HD 5005A	O4	V((fc))	OIII	145	178	65	52	84
HD 46223	O4	V((f))	OIII	119	240	58	58	94
HD 164794	O4	V((f))	OIII	113	228	55	55	94
HD 15629	O4.5	V((fc))	OIII	139	192	78	70	58
HD 192281	O4.5	Vn(f)	OIII	149	222	292	278	0
HD 46150	O5	V((f))z	OIII	104	277	66	73	93
HD 14434	O5.5	Vnn((f))p	OIII	287	244	430	430	172
HD 42088	O6	V((f))z	OIII	215	252	40	42	67
HD 167633	O6.5	V((f))	OIII	230	270	139	139	111
BD +62424	O6.5	V(n)((f))	OIII	237	214	48	53	85
HD 12993	O6.5	V((f))z	OIII	175	185	79	79	87
HD E228841	O6.5	Vn((f))	OIII	300	207	334	334	117
HD 168075	O7	V(n)((f))z	OIII	205	206	91	91	63
HD 47839	O7	V((f))var	OIII	205	391	39	43	66
HD 46573	O7	V((f))z	OIII	226	159	90	90	72
HD 36879	O7	V(n)((f))	OIII	285	248	219	219	54
HD 44811	O7	V(n)z	OIII	224	193	26	26	47
HD 217086	O7	Vnn((f))	OIII	314	226	399	379	59
HD 37022	O7	Vp	OIII	91	332	26	30	56
BD +60586A	O7	Vz	OIII	158	230	41	41	79
HD 46485	O7	Vn	OIII	351	225	326	326	114
HD 164492	O7.5	Vz	OIII	237	232	33	40	52
HD 53975	O7.5	Vz	OIII	240	224	180	180	45
HD 41997	O7.5	Vn((f))	OIII	256	255	265	265	39
HD 41161	O8	Vn	OIII	238	206	338	338	16
HD 191978	O8	Vz	OIII	263	257	62	56	81
HD 46056A	O8	Vn	OIII	304	179	377	377	113
HD 57236	O8.5	V	OIII	113	159	29	27	34
HD 46966	O8.5	IV	OIII	172	244	39	39	68
HD 52533	O8.5	IVn	OIII	169	158	301	286	181
HD 216532	O8.5	V((n))	OIII	204	243	203	203	30
HD 48279	O8.5	VNstrvar?	OIII	163	182	138	138	62
HD 214680	O9	V	OIII	179	404	16	16	41
HD 201345	ON9.5	IV	OIII	135	307	93	93	65
HD 192001	O9.5	IV	OIII	163	240	41	37	70
HD 57682	O9.5	IV	OIII	124	246	16	18	31
HD 149757	O9.5	IVnn	OIII	120	328	319	303	159
HD 36483	O9.5	IV(n)	OIII	175	167	180	180	45
HD 206183	O9.5	IV-V	OIII	85	322	13	11	25
HD 46202	O9.5	V	OIII	128	276	20	18	32
HD 12323	ON9.5	V	OIII	99	203	127	127	57
HD 34078	O9.5	V	OIII	116	236	13	14	30
HD 207538	O9.7	IV	OIII	84	288	30	27	52
HD 36512	O9.7	V	OIII	73	318	15	15	29
HD 54879	O9.7	V	OIII	58	170	8	6	10
HD 202214	O9.7	Vp	SiIII	139	207	15	15	29

Table A.4. Results from the `iacob-broad` analysis of the B dwarfs and subgiants (LC V and IV).

HD number	SpT	LC	Line	EW [mÅ]	S/N	$v \sin i$(FT) [km s^{-1}]	$v \sin i$(GOF) [km s^{-1}]	$v_{\rm m}$(GOF) [km s^{-1}]
HD 47417	B0	IV	SiIII	209	213	107	112	123
HD 37061	B0.2	V	SiIII	138	203	191	191	95
HD 36862	B0.5	V	SiIII	130	258	76	76	19
HD 36960	B0.5	V	SiIII	209	275	23	25	35
HD 37020	B0.5	V	SiIII	124	155	55	55	16
HD 144217	B0.5	V	SiIII	153	226	88	92	52
HD 201795	B0.7	V	SiIII	144	170	8	8	8
HD 37042	B0.7	V	SiIII	149	217	33	33	13
HD 36591	B1	IV	SiIII	175	290	9	9	18
HD 34989	B1	V	SiIII	142	218	48	48	16
HD 97991	B1	V	SiIII	159	167	144	144	36
HD 144470	B1	V((n))	SiIII	173	288	106	106	21
HD 28446B	B1	V	SiIII	173	199	12	10	24
HD 27192	B1.5	IV	SiIII	162	243	149	149	59
HD 37481	B1.5	IV	SiIII	143	278	74	74	14
HD 24640	B1.5	V	SiIII	128	218	119	125	83
HD 35299	B1.5	V	SiIII	136	233	8	4	15
HD 36351	B1.5	V	SiIII	139	212	29	29	14
HD 36959	B1.5	V	SiIII	142	240	12	11	12
HD 37744	B1.5	V	SiIII	140	296	37	37	15
HD 61068	B1	V	SiIII	168	213	12	11	24
HD 37209	B2	IV	SiIII	150	215	50	50	15
HD 36285	B2	IV-V	SiIII	113	156	11	9	18
HD 142669	B2	IV-V	SiIII	129	220	113	113	45
HD 3360	B2	IV	SiIII	147	215	23	23	17
HD 166182	B2	IV	SiIII	128	183	41	41	16
HD 3901	B2	V	SiIII	35	207	97	102	24
HD 35912	B2	V	SiIII	82	192	11	11	20
HD 36430	B2	V	SiIII	76	218	13	15	25
HD 36629	B2	V	SiIII	96	229	10	7	17
HD 144218	B2	V	SiIII	106	206	67	67	27
HD 120086	B2	V	SiIII	126	223	91	91	31
HD 37468D	B2	V	SiIII	136	233	202	202	60
HD 37479	B2	Vp	SiIII	94	164	170	153	85

Table A.5. Results from the `iacob-broad` analysis of the O and B stars identified as SB1.

HD number	SpT	LC	Line	EW [mÅ]	S/N	$v \sin i$(FT) [km s^{-1}]	$v \sin i$(GOF) [km s^{-1}]	$v_{\rm m}$(GOF) [km s^{-1}]
HD 199579	O6.5	V((f))z	OIII	211	215	49	54	79
HD 165921	O7	V	OIII	224	225	241	229	96
HD 35619	O7.5	V((f))	OIII	215	195	43	39	61
HD 191612	O8	f?pvar	OIII	129	321	45	40	69
HD 108	O8	f?pvar	OIII	228	314	43	47	82
HD 165246	O8	V(n)	OIII	258	249	261	261	52
HD 46149	O8.5	V	OIII	159	155	31	28	60
HD 14633	ON8.5	V	OIII	132	254	123	117	80
HD 57061	O9	II	OIII	260	223	90	90	72
HD 37043	O9	IIIvar	OIII	243	372	104	99	83
HD 193322A	O9	III	OIII	100	334	41	37	43
HD 163892	O9	IV((n))	OIII	188	259	206	206	72
HD 216898	O9	V	OIII	166	259	44	48	44
HD 36486	O9.5	IINwk	OIII	197	394	128	122	96
HD 93521	O9.5	IInn	OIII	155	216	380	380	133
HD 37366	O9.5	IV	OIII	95	184	18	13	39
HD 37041	O9.5	IVp	OIII	96	350	133	133	46
HD 25639	O9.5	V	OIII	161	226	234	234	58
HD 167264	O9.7	Iab	OIII	154	238	58	58	85
HD 6675	B0.2	III	SiIII	293	232	35	35	60
HD 36822	B0.2	IV	SiIII	229	218	19	20	36
HD 37023	B0.2	V	SiIII	82	223	48	48	12
HD 224151	B0.5	II-III	SiIII	309	178	132	132	39
HD 29248	B2	III	SiIII	224	298	32	34	40
HD 35039	B2	IV-V	SiIII	136	261	11	7	20
HD 104337	B2	IV	SiIII	178	180	99	99	49

Notes. The two O f?p stars, HD 108 and HD 191612, are also included in this table.